



Freie Universität Berlin  
Department of Earth Sciences  
Institute of Geological Sciences

## Masters's Thesis

---

# **Post-eruptive fan delta formation. Chaitén, Región de los Lagos, Chile**

**Date:** 29. Mai 2016

**Supervisors:** Prof. Dr. Alessandro Airo, Freie Universität Berlin  
Prof. Dr. Oliver Korup, Universität Potsdam

**Author:** Deniz Gök  
Mehringdamm 36  
10961 Berlin

Matriculation number: [4399610]

---

---

## Abstract

The 2008-2009 plinian eruptive phase of the Chaitén volcano in Chile (72.65 W, 42.85 S) caused a catastrophic sedimentary response within the adjacent southern catchment. Hydrology and morphology were deequilibrated due to the large input of volcaniclastic sediments. Pyroclastic density currents, hyperconcentrated flows and muddy stream flows have mobilized large quantities of sediment. The increased sediment yield caused channel avulsion in the lower part of the river Blanco and led to a catastrophic fan delta formation at the mouth of the newly formed river channel. DGPS surveys in 2014 and 2015 have been conducted to detect annual vertical changes of the delta. Ordinary Kriging interpolation was applied to create surfaces and calculate the annual volumetric change of  $7.8 \pm 2.5 \cdot 10^5 \text{ m}^3$ . The same dataset has been used to determine the minimum volume of the present delta of  $1.07 \pm 0.1 \cdot 10^7 \text{ m}^3$ . Sediment samples from the delta surface, pre-eruption channel, longshore dune and from deposits within the catchment were used to conclude erosional processes. Proximal samples from the catchment are more positively skewed and show smaller grain sizes than distal samples from the longshore dune or the delta plane. Kurtosis values of the longshore samples indicate that the origin of sorting is not caused by the depositional environment but rather a mirror of tidal reworking. A sediment budget on a catchment scale was set up by using an estimated minimum tephra input of  $2 \cdot 10^7 \text{ m}^3$  and a calculated sediment output of  $1.7 \pm 1.3 \cdot 10^7 \text{ m}^3$ . This results in a stored volume of  $0.3 \pm 1.3 \cdot 10^7 \text{ m}^3$  volcaniclastic sediments. The rhyolitic eruption caused a specific sediment yield of  $5.4 \pm 0.5 \cdot 10^4 \text{ t km}^{-2} \text{ yr}^{-1}$  and thus can be defined as an extreme event. The Chaitén delta would persist  $14 \pm 3$  years, assuming volume decrease is mainly controlled by remaining cycling erosional processes (e.g. tides, waves, rainfall) on a moderate time scale. Measuring 16 deltas in southern Chile by remote sensing and calculating the related catchment size indicates that volcanic eruptions disturb the scaling relation on a short-term scale.

---

## **Declaration of originality**

I hereby declare that the thesis entitled,  
*Post-eruptive fan delta formation. Chaitén, Región de los Lagos, Chile*  
is my own original work carried out as a Master's student at the Freie Universität Berlin.  
All sources used for the thesis have been fully and properly cited. This thesis was neither  
in the same nor in a similar way part of any other academic examination.

Signature \_\_\_\_\_

---

## Acknowledgements

I would first like to thank my thesis advisors Prof. Dr. Oliver Korup from the Institute of Earth and Environmental Science at Universität Potsdam and Prof. Dr. Alessandro Airo from the Institute of Geological Sciences at Freie Universität Berlin. Both doors to their offices have always been open whenever I ran into a trouble spot or had a question about my research or writing. Prof. Korup and also Dr. Christian Mohr from Universität Potsdam gave me the possibility to participate in three wonderful field trips even though I am an external student. Thank you!

I would particularly like to thank Prof. Dr. Andrés Iroumé, Dr. Hector Ulloa and Daniel Antileo for all the support before, during and after the field trips. They always made me feel to be part of something bigger.

Furthermore I would like to thank some projects and foundations. The field trips to Chaitén would not have been possible without the financial support of the CONICYT-BMBF project PCCI20130045 and the PROMOS scholarships from Freie Universität. Also I would like to thank the Keller-Budenberg-Stiftung and the Charlotte-Schimmelpfennig-Stiftung for their scholarships within the last year.

## Contents

<b>1</b>	<b>Introduction</b>	<b>8</b>
1.1	Sedimentary response to volcanic eruptions . . . . .	8
1.2	Global overview of sediment yields . . . . .	10
1.3	Chaitén: Problem statement and objective . . . . .	10
<b>2</b>	<b>Study area</b>	<b>13</b>
2.1	Geological background . . . . .	14
2.2	Avulsion and Delta formation . . . . .	16
<b>3</b>	<b>Methodology</b>	<b>18</b>
3.1	Field work . . . . .	18
3.2	Laboratory work . . . . .	22
3.2.1	Grain size analysis . . . . .	22
3.3	Data analysis . . . . .	22
3.3.1	DGPS data interpolation and surface generation . . . . .	22
3.3.2	Volume difference . . . . .	25
3.3.3	Granulometry . . . . .	25
<b>4</b>	<b>Results</b>	<b>28</b>
4.1	Chaitén Delta changes between 2014 and 2015 . . . . .	28
4.2	Sediment characteristics . . . . .	29
4.3	Sediment Budget . . . . .	36
<b>5</b>	<b>Discussion</b>	<b>38</b>
<b>6</b>	<b>Conclusion</b>	<b>50</b>
<b>References</b>		<b>55</b>
<b>Appendix</b>		<b>-56</b>
<b>A Programming code in R</b>		<b>A-1</b>
<b>B Figures</b>		<b>B-1</b>
<b>C Data of delta comparision</b>		<b>C-1</b>
<b>D Grain size data</b>		<b>D-1</b>

## List of Figures

1	Schematic volcanogenic sediment budget after (Pierson and Major, 2014) . . . . .	9
2	Extreme specific sediment yields . . . . .	10
3	Publications on volcanic deltas . . . . .	11
4	Overview map of Chile, the Region 10 and the Chaitén drainage basin . . . . .	13
5	Rocktypes . . . . .	14
6	Geological map of Chaitén region . . . . .	15
7	Panorama view of the Chaitén Delta . . . . .	16
8	Present day setting of the Chaitén coastline . . . . .	17
9	DGPS data points . . . . .	18
10	DGPS Equipment . . . . .	19
11	Sediment sampling . . . . .	20
12	Sediment sample locations of longshore dune, delta plane and pre-eruption channel	21
13	Semivariograms delta 2 . . . . .	23
14	Semivariograms delta 1 . . . . .	24
15	Interpolated DGPS data (delta 2) . . . . .	24
16	Interpolated DGPS data (delta 2) . . . . .	25
17	Elevation difference of the interpolated DGPS data . . . . .	28
18	Grain size statistics (mean and sorting) . . . . .	30
19	Grain size statistics (skewness and kurtosis) . . . . .	31
20	Subdivisions of river systems . . . . .	37
21	Density plots of the DGPS data . . . . .	38
22	Sensitivity test delta 2 . . . . .	39
23	Sensitivity test delta 1 . . . . .	40
24	Delta profile transects . . . . .	42
25	Elevation profiles delta 2 . . . . .	43
26	Elevation profiles delta 1 . . . . .	43
27	Density plots of mean values . . . . .	45
28	Calculation of total inflow volume . . . . .	47
29	Relation of delta area to catchment area . . . . .	49
30	Elevation difference of the interpolated DGPS data . . . . .	B-1
31	Density plot of the statistical parameters mean . . . . .	B-2
32	Density plot of the statistical parameter sorting . . . . .	B-2
33	Density plot of the statistical parameter skewness . . . . .	B-3
34	Density plot of the statistical parameter kurtosis . . . . .	B-3
35	Greenschist bed load sample . . . . .	B-4
36	Granodiorite bed load sample . . . . .	B-4
37	Rhyolite bed load sample . . . . .	B-5

**List of Tables**

1	Meshsizes in mm . . . . .	22
2	Parameters to describe the semivariogram . . . . .	23
3	Ranges of $\phi$ values and associated descriptions . . . . .	27
4	Results grain size analysis 2013 delta samples . . . . .	32
5	Results grain size analysis 2013 catchment samples . . . . .	33
6	Results grain size analysis 2015 longshore samples . . . . .	34
7	Results grain size analysis 2014 pre-eruption channel samples . . . . .	35
8	Main physical parameters . . . . .	37
9	Data of delta comparison . . . . .	C-1
10	General information of sediment sampling . . . . .	D-1
11	Sample mass and sieving loss . . . . .	D-2
12	Grain size data of the 2013 delta samples . . . . .	D-3
13	Grain size data of the 2014 pre-eruption samples . . . . .	D-4
14	Grain size data of the 2015 catchment samples . . . . .	D-5
15	Grain size data of the 2015 longshore samples . . . . .	D-6

## 1 Introduction

### 1.1 Sedimentary response to volcanic eruptions

Explosive volcanic eruptions produce large quantities of volcaniclastic sediments with the ability to change landscapes on a long-term time scale. Sometimes the consequences of disturbed landscapes have a greater socioeconomic impact than the eruption itself (Pierson and Major, 2014). Volcaniclastic sediments are clastic deposits derived from the transport, deposition and/or redeposition of the products of volcanic activity (Manville et al., 2009). This additional sediment input into drainage networks causes various morphological changes. Highly erodible, unconsolidated, volcaniclastic sediments can cause 1) aggrading river channels, 2) development of new hydrological channels, 3) rapid erosion of hillslopes and flanks, mantled by tephra, 4) damming lakes from rivers and 5) avalanches of volcaniclastic sediments. The main sedimentary processes related to plinian eruptions which cause hydrogeomorphic responses on a catchment scale are tephra fall, pyroclastic density currents (PDC), pyroclastic surges, debris avalanches and hyperconcentrated flows/ lahars. The dimension of disturbance scales generally with the magnitude of the eruption, the type transport process and distance to the vent (Pierson and Major, 2014; Manville et al., 2009).

Tephra fall, fine volcaniclastic particles transported by wind after an explosive eruption, can reach regions far distant from vent and causes changes in hydrology and sedimentation. Due to physical and/or chemical interactions, it can kill, damage or bury vegetation and continuously mantles hillslopes and flanks. The deposits are highly erodible and can easily be remobilized by rainstorms. Hillslope mantling of fine grained tephra fall increases surface runoff due to impermeability of the sediments (Pierson and Major, 2014).

Debris avalanches are formed when an unstable slope collapses and debris is transported away from the slope. Large scale avalanches normally occur on very steep volcanoes. There are two general types of debris avalanches: Those that are "cold" and those that are "hot". A cold debris avalanche usually results from a slope becoming unstable whereas a hot debris avalanche is the result of volcanic activity such as volcanic earthquakes or injection of magma which causes slope instability. Deposits can reach volumes up to  $1 \text{ km}^3$  and are able to block complete tributary valleys (Siebert, 2002). The commonly fan shaped deposits can provide a long-term sediment supply of a fluvial system.

The most spectacular phenomena of explosives eruptions are PDCs resulting from collapsing ash columns. These highly destructive gravity-driven mixtures of hot gas and volcanic rock fragments of all sizes can reach temperatures of  $100 - 700^\circ\text{C}$ . The fast moving rock particles can exceed velocities of several hundred  $\text{m s}^{-1}$  (Branney and Kokelaar, 2002) and emplace volume greater  $1 \text{ km}^3$ . The geomorphic impact is often catastrophic, vegetation and even soils can be stripped of from hillslopes and small watersheds can be rearranged by the deposition of the pyroclastic material. Similar to debris avalanches, deposits from PDCs can provide a long-term sediment supply.

Non cohesive debris avalanches in humid climates tend to dilute and transform to lahars

through mixing with ambient stream water or sediment loss by partial deposition (Manville et al., 2009). But also deposits from tephra fall or PDCs in combination with heavy rainfall can generate lahars. Thus, lahars are secondary processes of volcanic activity and can be triggered by rainfalls years after an eruption. The impact is usually focused along river channels (Pierson and Major, 2014) but can damage surrounding vegetation. Travel distances of lahars are commonly 10 – 30 km but can reach up to > 100 km in some cases before they evolve into muddy water flows (Pierson et al., 1992). Deposits often provide a moderate-term sediment supply to fluvial systems.

All deposits of the mentioned processes accumulate on hillslopes, in valley floors or directly into streams and change the boundary conditions regarding mass and water fluxes. On a long-term timescale the generation and deposition of sediments must balance to reach steady state (Sadler and Jerolmack, 2015). In a volcanically disturbed catchment, the volumetric amount of sediment leaving the drainage basin and the amount stored sediment within the basin (e.g. in terraces, channels or on hillslopes) must equal the amount of sediment delivered into the catchment by the eruption. This concept of a simplified sediment budget is given by the equation:

$$I = \Delta S + O \quad (1)$$

Where  $I$  is the sediment input,  $\Delta S$  the sediment storage and  $O$  the sediment output. Figure 1 shows an example of the schematic distribution of volcaniclastic sediment volumes by different transport processes.

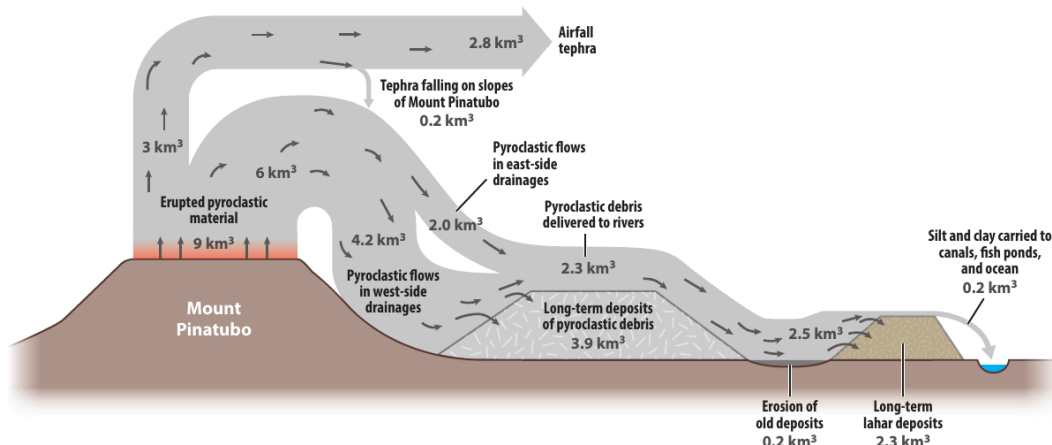


**Figure 1:** Schematic volcanogenic sediment budget after (Pierson and Major, 2014)

## 1.2 Global overview of sediment yields

The highest volumetric amounts of volcaniclastic sediments are mobilized on convergent plate margins. Fore-arc and back-arc basins contain the most volcaniclastic materials due to the proximity to volcanic arcs (Manville et al., 2009). Other impactors which produce or rise significant sediment fluxes in mountain rivers on a global scale are earthquake- and storm triggered landslides, dam breaks and glaciers. Korup (2012) reviewed the highest reported specific sediment yields impacted by the mentioned factors. Figure 2 shows the specific sediment yields which exceed the 95th percentile of the compiled data and therefore was defined as *extreme* yields. Magnitudes range between  $10^4 \text{ t km}^{-2}\text{yr}^{-1}$  and  $10^7 \text{ t km}^{-2}\text{yr}^{-1}$  for a given minimal reference interval of one year.

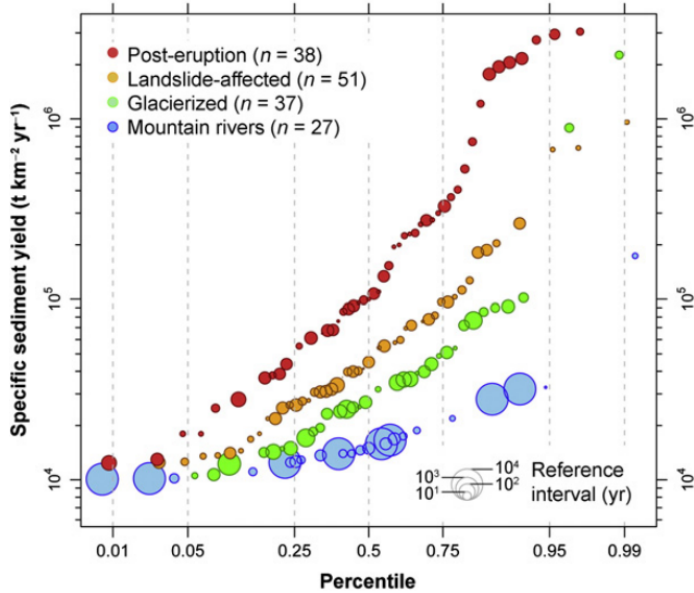


**Figure 2:** Extreme specific sediment yields (Korup, 2012)

Figure 2 shows that post-eruptive sedimentation processes produce the highest fluxes on global sedimentation.

## 1.3 Chaitén: Problem statement and objective

Rhyolitic eruptions are the most explosives volcanic eruptions on earth due to the high amount of silica and therefore the high viscosity of the magma. The recurrence intervals of 100 to 100000 years of those eruptions are the reason why only a few observations are known (Pallister et al., 2010).

The rhyolitic 2008 eruption of the Chaitén volcano in southern Chile was followed by a rapid sedimentary response which deequilibrated hydrology and morphology of at least two catchments adjacent to the vent of Chaitén volcano. This thesis investigates the sedimentary consequences in the southern catchment which drains by the river Blanco southwest next to the town Chaitén. Extremely high amounts of volcaniclastic sediments were deposited to the catchment and changed the behavior of the Blanco river.

Pyroclastic density currents, tephra fall and lahars increased the transport capacity of the river and caused rapid channel bed aggradation. As a consequence the lower part of the Blanco river avulsed and formed a new channel through Chaitén city. The sediment masses, mostly transported by lahars, created a volcaniclastic delta at the shoreline of Chaitén town and increased the already existent delta south of the town.

Literature provides little information of the short- and long-term effects of volcanogenic delta formation. In general the investigation of non-volcanic deltas is led by the hydrocarbon industry and scientific sedimentology. ScienceDirect.com provides 2350 publications from planetary and earth science within the last 10 years including the keywords *delta* and *sedimentology*. Only 339 publications by adding *volcano* as a search parameter (Fig 3). Many geoscientific publications are published regarding the development and evolution of deltaic systems but very few authors are working on volcanogenic deltas.

Morphology and facies of conventional deltas are mainly controlled by climate, tectonics, topography, subsidence and eustatic sea level (Postma, 1990). These factors influence both the 1) fluvial system which feeds the deltaic system by a certain amount sediment load and 2) the depositional system in the target basin in terms of bathymetry, waves and tide. Sedimentary facies of deltas show a decrease of grain size with increasing distance from channel mouth because the decrease of stream velocity results in deposition of the coarser sediment load. Furthermore sequence stratigraphy plays an important role in delta analysis. It is to distinguish whether the incoming sediment was deposited in a transgressive or regressive phase to interpret the architecture of the sediment body (Catuneanu, 2006). Thus, the evolution of non-volcanogenic deltas is controlled by highly time consuming processes while volcanogenic deltas result from extremely rapid and pulsed sedimentation of highly erodible material. This difference is relevant regarding the persistence time of such a sediment body. Once the deposition of transported material after an eruption begins, the delta gets modified by waves, tide, wind and fluvial erosion. Volcaniclastic sediments following rhyolitic plinian eruptions consist of pumice (very low density), microcrystalline rhyolite, obsidian and wall rock (Alfano et al., 2011). Especially the pumice fraction leads to a high erodibility of those types of sediments.

I hypothesize that the Chaitén delta is volumetrically still growing and gets fed by observed volcaniclastic deposits in the upper part of the Blanco river. This implicates that the rate of sediment supply from stored deposits and the rate of erosion from the existent delta are

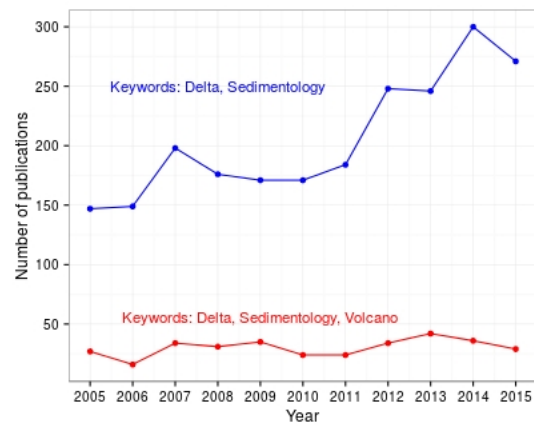


**Figure 3:** Search results of ScienceDirect.com from 2005 to present in planetary and earth science

not acting on the same time scale.

Previous publications on the Chaitén eruption have shown that around  $0.5 - 1.0 \cdot 10^9 \text{ m}^3$  of tephra was ejected by the eruption (Alfano et al., 2011). Pierson et al. (2013) estimated the minimum tephra volume that entered the Chaitén catchment to be  $2.0 \cdot 10^7 \text{ m}^3$  on basis of Alfano et al. (2011). A  $3 \cdot 10^6 \text{ m}^2$  deltaic area formed as a consequence of the extraordinary high sediment supply. The objectives of this study are to quantify the annual volumetric change of the Chaitén delta by conducted DGPS (Differential Global Positioning System) surveys in 2014 and 2015 and to set up a simplified sediment mass balance using the estimations of Pierson et al. (2013) and Alfano et al. (2011). Furthermore grain size analysis will be used to conclude the persistence time of the delta.

This leads to following research questions:

1. Does the Chaitén Delta change volumetrically over time?
2. How long will the Chaitén Delta persist?
3. How much Sediment is still stored within the Chaitén catchment?
4. How relevant was the sedimentary impact of the 2008 eruption in relation to global extreme sediment yields?

## 2 Study area

The Chaitén volcano, located in southern Chile (72.65 W, 42.85 S), is part of the region X, called “Region de los Lagos”. The volcano is located at the edge of two main catchments. The northern one, which is also the drainage basin of the much larger volcano Michinmahuida and the southern one which is the area of interest in this thesis. The catchment (Fig. 4) measures 77 km<sup>2</sup> and forms the drainage network of the river Blanco (*Rio Blanco*). The river Blanco flows from the southern flank of Chaitén volcano southwestwards through Chaitén town into the Gulf of Corcovado. The town Chaitén, 10 km away from the volcano was strongly affected by the morphological sedimentary response due to the 2008 eruption.



**Figure 4:** Overview map of Chile, the Region 10 and the Chaitén drainage basin

The region is climatically characterized by the valdivian rainforest, a cold temperate ecosystem with a mean annual ground surface temperature of 11-12° C (Veblen et al., 2015). Western Patagonia shows climatically hyperhumid conditions with annual precipitation

ranges between 5000 and 10000 mm. It belongs to the most intensely rainfall regions worldwide (Garreaud et al., 2013). Between 30° and 60° latitude, climate is strongly influenced by the westerlies. The water saturated air from the Pacific Ocean condenses on the western flanks of the Andes and produces heavy rainfalls (Stuut et al., 2006). A high landscape relief, a high amount of water and an active sediment source are leading to extreme surface processes and rapid morphological changes controlled by erosion and sedimentation.

## 2.1 Geological background

The geological map (Fig. 6) contains the combined information of Servicio Nacional de Geología y Minería (2002); Encinas et al. (2014). The geology in this region is poorly known because the vegetation often confines the exposure of outcrops. The geological map is quite detailed but the reliability of some interpretations is doubtful. Encinas et al. (2014) has shown some uncertainties within the longitudinal depression between the Coastal Cordillera and the Main Andean Cordillera. A GIS based web application from Servicio Nacional de Geología y Minería (2002) provides a more detailed geological map of the region which in some points disagrees with Encinas. Nevertheless the coincident parts have been combined and small details are based on SERNAGEOMIN informations.

Within the catchment of the study area the geology is dominated by Miocene igneous rocks, Pleistocene to Triassic metamorphic rocks and Pleistocene to Holocene volcanic rocks. Valley fill of the catchment shows fluvial, alluvial, deltaic and litoral sedimentary deposits from Pleistocene to Holocene. A north- south orientated sinistral strike slip fault is located in the eastern part of the map.

Basically three types of rocks can be found near Chaitén: metamorphic rocks, igneous rocks and volcanic rocks. Handrock samples from the Chaitén catchment (Fig. 5) confirms the informations of the geological map. Bed load of the river Blanco is mainly composed of the mentioned rock types (enlarged figures attached).

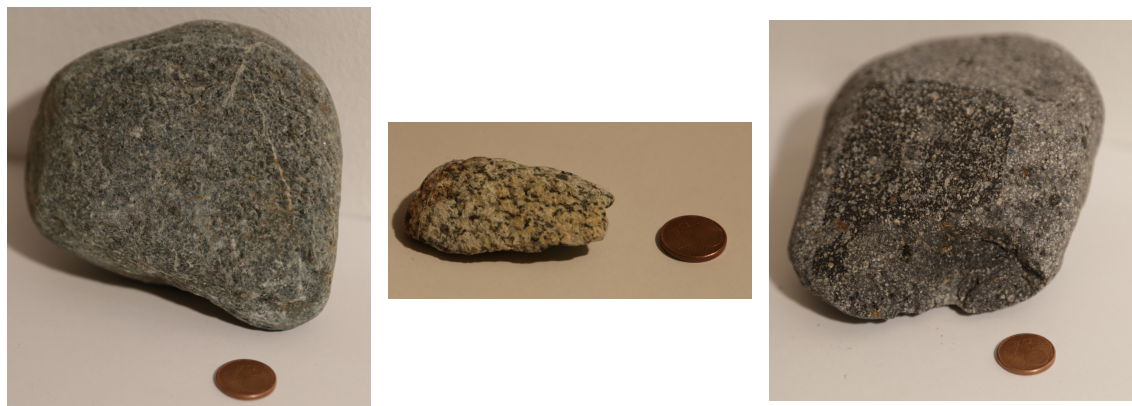


**Figure 5:** A) metamorphic rock (Greenschist), B) igneous rock (Granodiorite) and C) volcanic rock (Rhyolite)

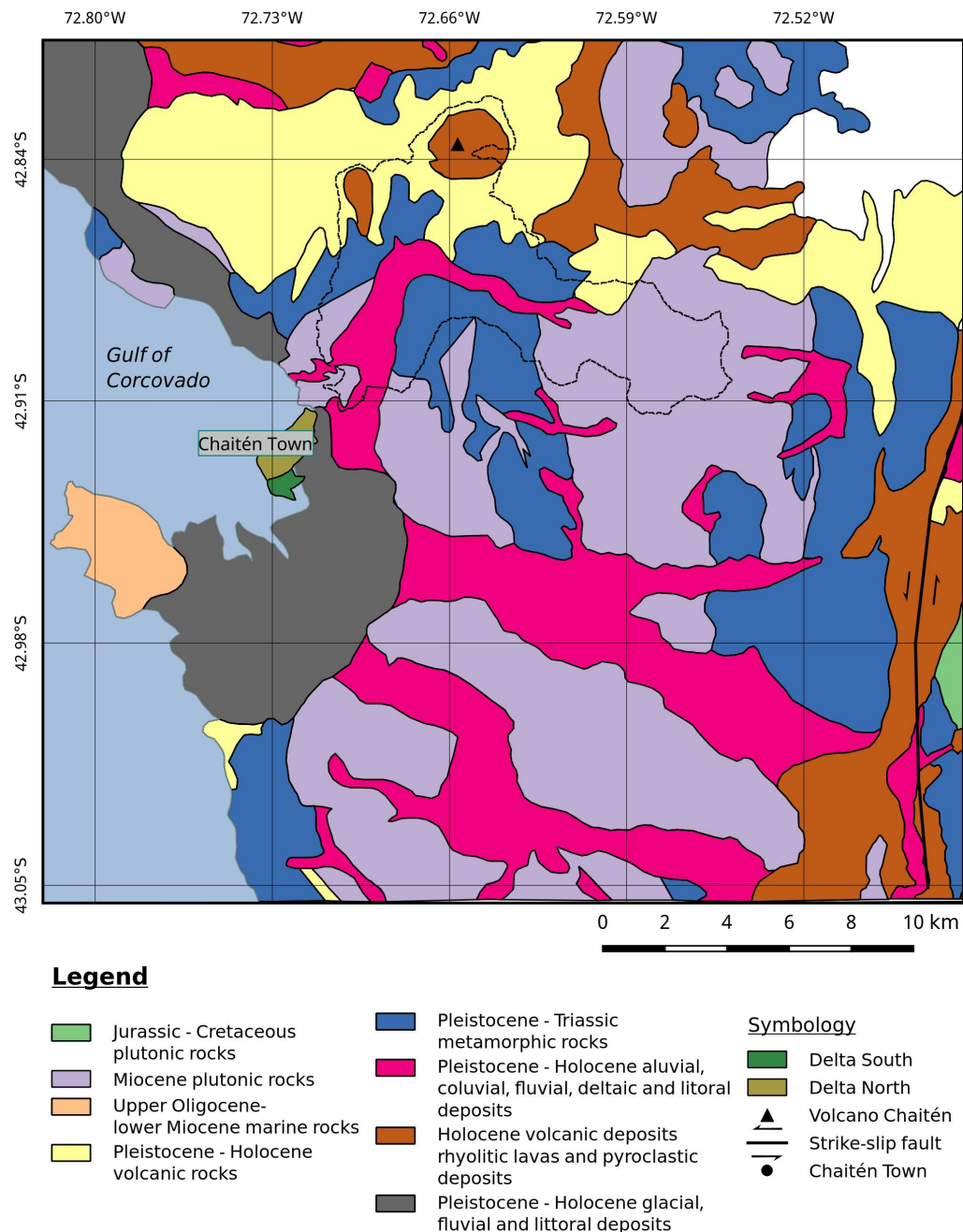


**Figure 6:** Geological map of Chaitén region. Modified after Servicio Nacional de Geología y Minería (2002) and Encinas et al. (2014)

The eruption history of the Chaitén volcano shows that the first verified eruption occurred  $7750 \text{ BC} \pm 200$  years based on radiocarbon dating. The second eruption occurred  $6650 \text{ BC} \pm 1300$  years and had a volcanic explosivity index (VEI) of 5. This eruption was dated by a tephrochronology analysis. Further eruptions with an explosivity of VEI 4 have been detected around  $3100 \text{ BC} \pm 1300$  years and  $1640 \pm 18$  years. Than in 2008 followed the last documented eruption. By taking the error ranges into account follows an average eruption recurrence of  $1950 \pm 550$  years although five data points do not provide a basis for a reliable statistic.

## 2.2 Avulsion and Delta formation



**Figure 7:** Panorama view of the Chaitén Delta

The 2008-2009 eruptive phase of the Chaitén volcano caused various sedimentary responses in the catchment of the Blanco river. A detailed eruption chronology was omitted because several authors already summarised the events the the related timing (Umazano et al., 2014; Pierson et al., 2013; Major et al., 2013; Major and Lara, 2013; Lara, 2009). Nevertheless a short process-based succession of the sedimentary responses is necessary to understand the environmental and social impact of this event.

A continuously rising eruption column, due to the initial eruption, caused a wide distribution of fine tephra way beyond the adjacent catchment. During the rise of the column various small PDCs occurred primarily within the caldera and subsequently into the drainage basin. Heavy forest disturbance and biomass mobilisation were the consequence. Continuous heavy rainfall started to erode the deposits from hillslope mantling tephra and PDCs. The additional sediment supply caused high channel bed aggregation of the Blanco river. Hyperconcentrated flows began to form. The accommodation space of the former channel was filled by volcaniclastic sediments and caused overbank flooding. Avulsion of the lowermost part of the Blanco river led to heavy destruction of Chaitén City. Delta growth of the northern delta began (Fig. 8) after the southern delta could not compensate the large sediment masses.

Figure 8 shows a Google Satellite image and schematic sketch of the deltaic area in Chaitén. The pre-eruption channel (black) shows the former channel path to the primary formed delta (Delta 1). This southern delta measures around  $1 \text{ km}^2$  while the northern delta (delta 2) is about  $2 \text{ km}^2$ . The no-data area is also part of delta 2. Incision and sedimentation of the river on delta 2 caused channel switching several times during the last eight years and flows currently through the southern part of delta 2.

Nearly 90% of the Chaitén town has been flooded a few days after the eruption and the infrastructure was buried up to 3 meters by the deposition of volcaniclastic sediments.

Transported woody and lithic debris damaged buildings through direct impacts and some buildings have been lifted up and were transported into the delta plain. The small Chaitén

airport had to be closed because the runway was also buried by sediments.

The present-day situation allows an easy access to the delta plane by foot and by car, however it is not recommendable to get close to the channel by car. Large woody debris was transported by the lahar impulses into the delta and gets nowadays collected as firewood. Hence, there is a certain anthropogenic impact on the delta surface.

Pierson et al. (2013) estimated that the volume of delta 1 (the original Chaitén delta) is about  $1 - 3 \cdot 10^6 \text{ m}^3$  and the lahar deposits within the pre-eruption channel measure  $0.8 - 1 \cdot 10^6 \text{ m}^3$ . Peak discharge of the flow before avulsion occurred could have been around  $350 - 550 \text{ m}^3 \text{ s}^{-1}$  Pierson et al. (2013).

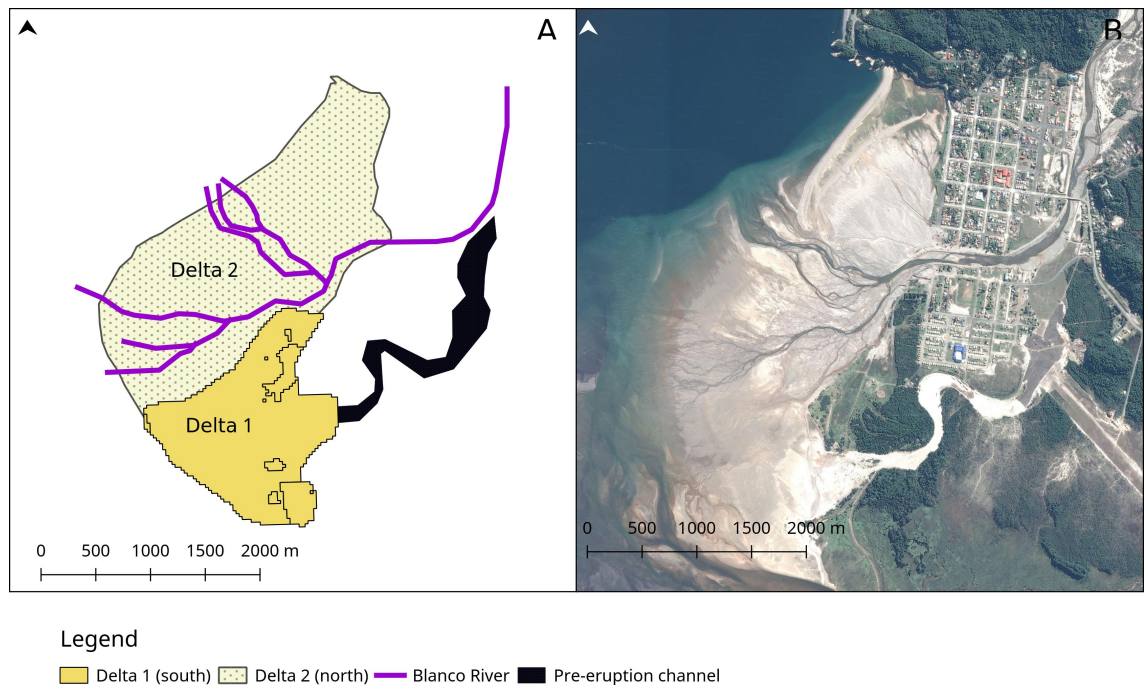


**Figure 8:** Schematic drawing of pre-eruption channel, both deltas and a Google Satellite Image (2016)

### 3 Methodology

This study combines field measurements and sampling with laboratory work and computational data analysis. Remote sensing techniques have been used to compare the Chaitén Delta qualitatively with similar morphological structures in Patagonia. Field trips for sediment sampling and DGPS (Differential Global Positioning System) measurements were conducted in February 2014 and March 2015.

#### 3.1 Field work

##### DGPS measurements

Two DGPS surveys were conducted in February 2014 and March 2015 to measure the elevation of the Chaitén delta. Measurements were conducted in both the southern (delta 1) and the northern delta (delta 2) and delivered more than 1000 GPS points per year for each delta. A Trimble R5 DGPS with two double frequency L1/L2 (P) receiver (Fig. 10) was used. The systematic error of this equipment is 20 mm (vertical and horizontal). The horizontal error was neglected because the area of the deltas plane was derived from satellite images and not from the DGPS data. Furthermore this error has no significant influence on the volume difference but rather would result only in a slightly different elevation pattern. The vertical error of the DGPS was considered.

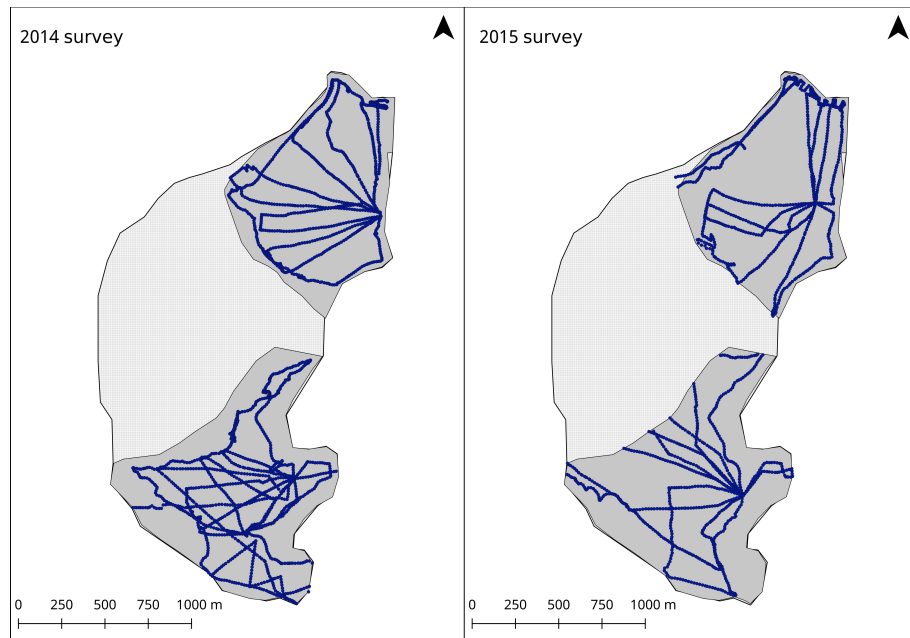


**Figure 9:** DGPS data points from 2014 survey (left) and DGPS data points from 2015 survey (right)

Figure (9) shows a simplified map of delta 1 and delta 2 with both datasets from 2014 and 2015. The survey was conducted continuously in a 40 seconds time interval. The measurements were done by foot on transectional paths to cover a wide range of the area. Hence, a high resolution could be recorded and formed the basis for a digital elevation model of the deltas. The no-data region (Fig. 9) of both surveys belongs to delta 2 and was not accessible

in the time of measurement due to flooding of the area or widely spread channels of the river.

The DGPS base station (Fig. 10) was installed on a known position to receive a GNSS signal of satellites which contain positional errors due to atmospheric interferences. Because the position is known, the error solution of the signal can be calculated and sent out to the mobile antenna by the base station. Hence, the mobile DGPS is able to correct the position in real time and delivers highly accurate position and elevation data. Post-processing of the raw data to correct the errors was done by the chilean partners of *Universidad Austral de Chile* using the Trimble Business Center software.

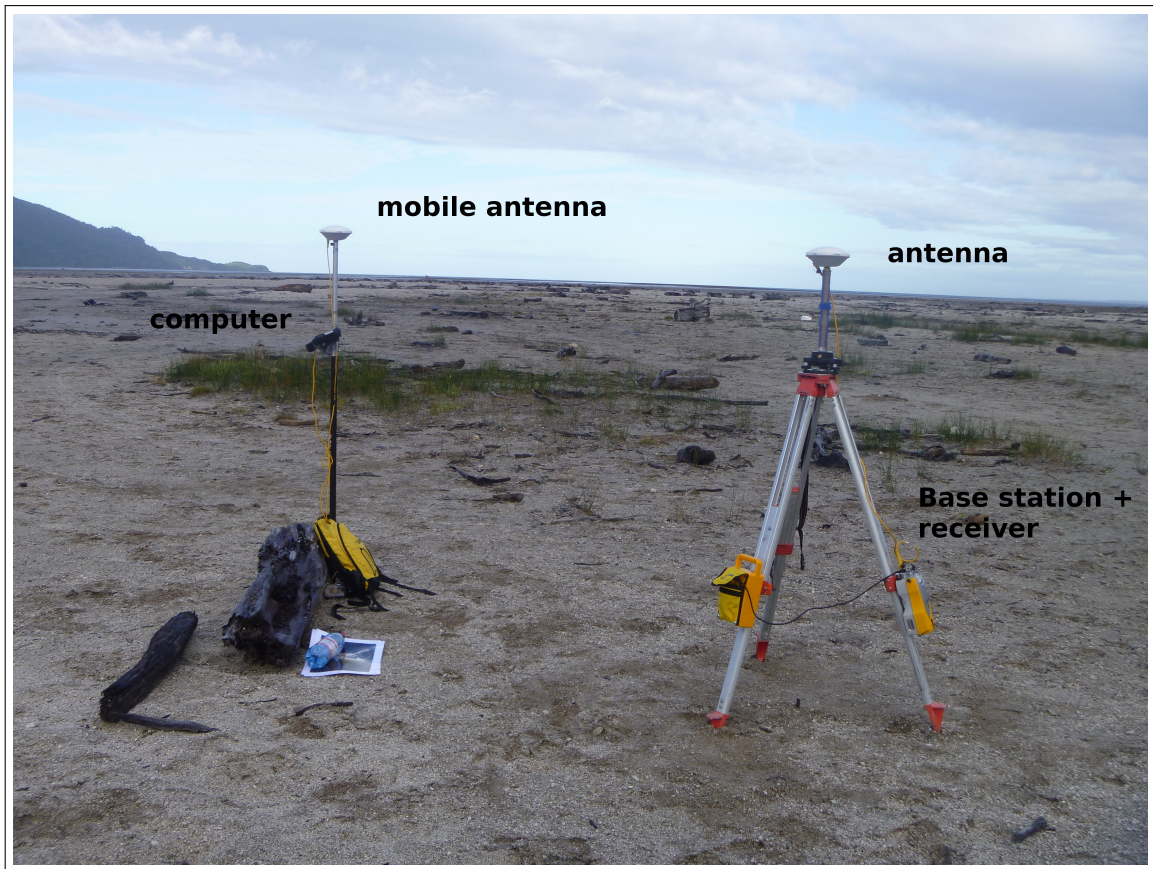


**Figure 10:** DGPS Equipment (view in southern direction of delta 1)

### Sediment sampling

Sediment sampling was done in four different depositional environments (Fig. 12). In total 70 samples split in 19 samples from the delta plane, 10 samples from the pre-eruption channel, 16 samples from terraces within the catchment and 25 samples from the longshore dune. The samples from delta plane, pre-eruption channel and the longshore dune were taken from the surface and the sample size was between 500g and 1200g for each sample (details attached). There was no vertical stratification noticeable within the first half meter of the accumulations and it was not expected because deposition of the material occurred pulsed and catastrophic. The samples from stream terrace deposits were taken directly out

of the layer (Fig. 11) because surface was not accessible at all sampling sites. The samples have not strongly been influenced by erosional processes because there was no longtime exposure to the surface. An initial lahar deposit composition was expected and should be used to compare the results with a more distal depositional environment. Therefore the nested sampling method was used to reduce uncertainties. Nested sampling means to sample from each sample location several sub-samples within one square meter. The longshore dune was sampled using the same method because the erosion by tidal energy and waves was expected to be high. Five sub-samples from the longshore dune have been taken on each of the five sample locations to obtain statistically higher accuracy. The 2013 samples from the delta plane and the 2014 samples from the pre-eruption channel were taken from the surface. Single samples for both sample locations. The surfaces of both depositional environments are influenced by rain, wind, incision channels and the anthropogenic impact. Therefore the priority of the sampling was to obtain a widely spread area.



**Figure 11:** Sediment sampling surface (left) and sampling from terrace deposit (right)

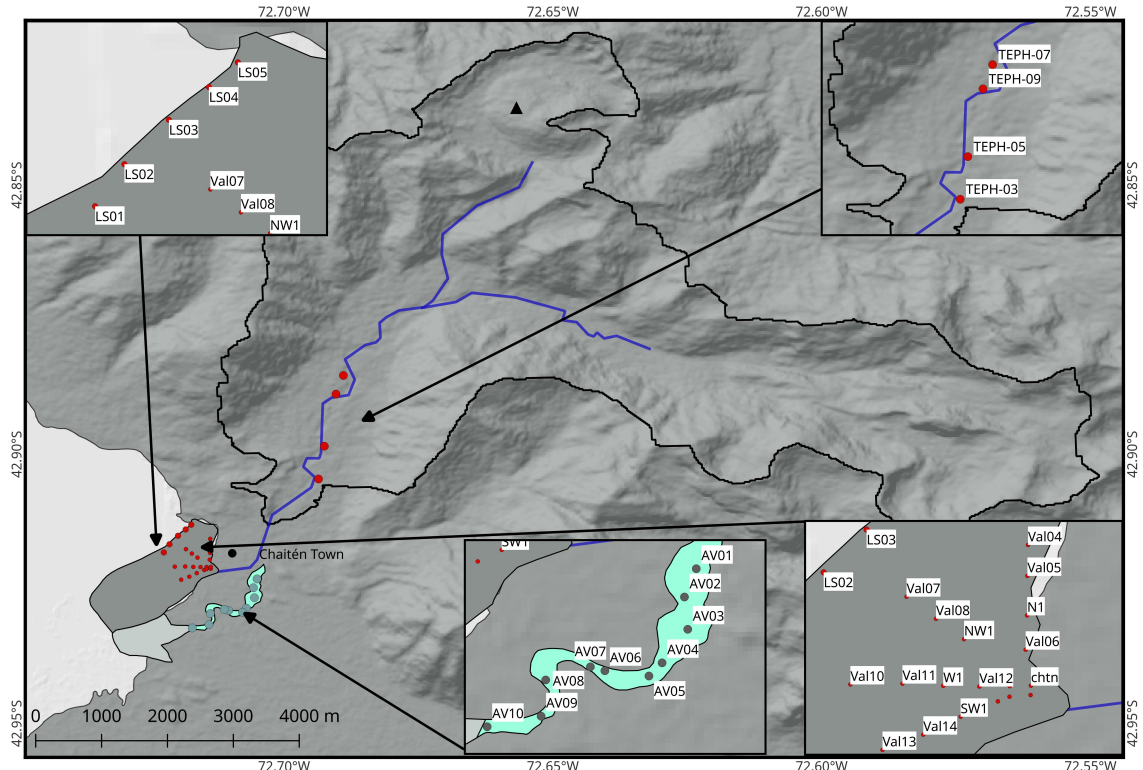


**Figure 12:** Sediment sample locations of longshore dune, delta plane and pre-eruption channel

Granulometric data of the transectional sediment samples (Fig. 12) from a previous field trip in January 2013 was used to have a more comprehensive database. Samples have been taken from delta plane in four transects (north, northwest, west and southwest) to examine granulometric behavoir in radial distance from channel mouth. In this study the internal variation in grain size characteristics is of secondary interest. Variations of granulometric parameters in the four different depositional environments is the focal point of interest. All sample locations are plotted in Fig. 12 and listed attached.

### 3.2 Laboratory work

#### 3.2.1 Grain size analysis

Sediment samples have been processed at both the *Universidad Austral de Chile (UACH)* and the sediment laboratory of *Freie Universität Berlin*. All samples have been prepared in Chile, this included drying at 105°C for at least 24 hours and weighting of all sediment samples. The mesh sizes of the sieves available at the chilean university were slightly different than at Freie Universität Berlin. The used sieve sizes are listed in Table 1. The absolute weight, the cumulative weight and the loss of sediment fraction of each sample can be found in the attachment.

**Table 1:** Meshsizes in mm

UACH	10	6,3	4,00	2	1,00	0,6	0,425	0,212	0,125	0,063
FU Berlin	10	6,3	3,15	2	1,25	0,6	0,400	0,250	0,125	0,063

### 3.3 Data analysis

All data analysis was done by using the open source R software environment. The required packages and used scripts can be found in the attachment.

#### 3.3.1 DGPS data interpolation and surface generation

The datasets from the DGPS measurements in 2014 involve 2293 points (1073 for delta 2 and 1225 for delta 1). From the survey in 2015 were 1706 points recorded (930 in the northern delta and 776 in the southern delta). A 20m x 20m mesh size grid for the interpolation was used to cover the area of the delta. The gridded area was cropped with a shapefile from the delta to obtain raster surfaces from the datasets. The elevation data of both surveys was spatially reprojected. The applied system (spatial reference system 32718) contains the geodetic reference ellipsoid WGS 1984 with an UTM (Universal Transverse Mercator) 18S projection.

The used geostatistical interpolation method is called *ordinary Kriging* and delivered the most reasonable results. Ordinary Kriging interpolation respects the distance between known data points and the degree of variation between them to estimate values in unknown areas. Therefore the nearby known data points have to be weighted for each unknown point (each grid cell within the interpolation area). Ordinary Kriging provides the possibility to create a semivariogram to receive the best possible and most unbiased weighting results. Modelling a semivariogram means to find the relationship between the DGPS point locations to identify the variability of the measurement (in this case elevation) with distance. Once the variance in elevation with distance between all DGPS locations is (e.g. graphically) represented, it is possible to fit a statistical model.

Figure 13 and 14 show the semivariograms for both datasets from 2014 and 2015 in delta 1 and delta 2. The describing parameters to process ordinary Kriging have been chosen from

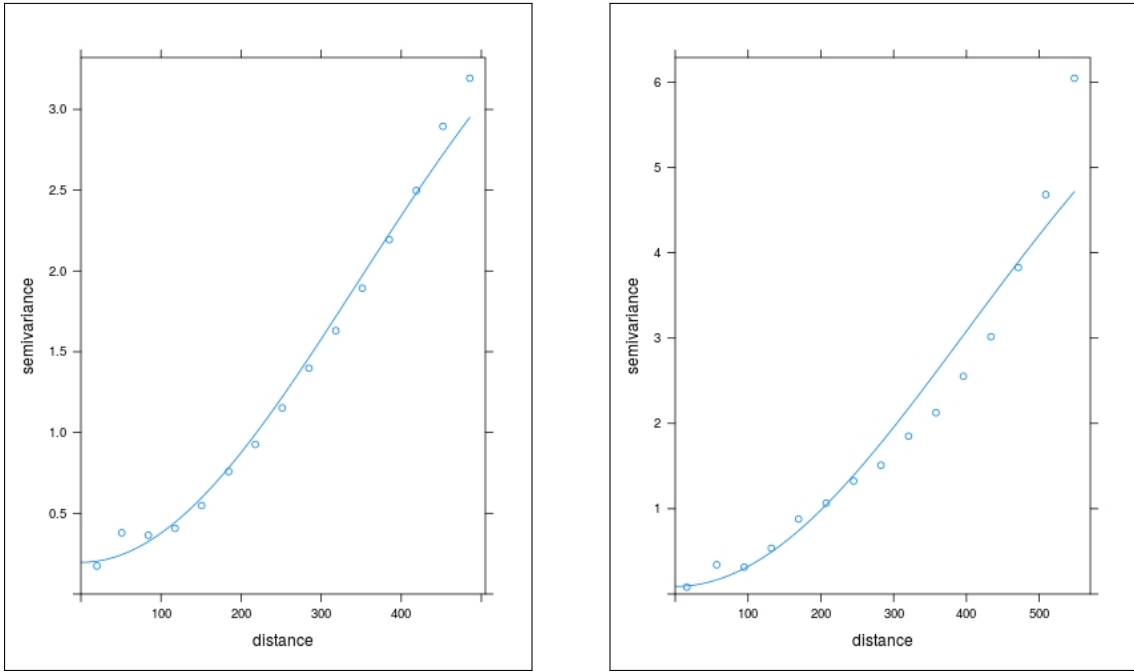


**Figure 13:** Semivariograms of the northern delta from 2014 (left) and 2015 (right)

the calculated variogram and are called *Range*, *Sill* and *Nugget*. The nugget describes the point on the y-axis where the semivariance starts (axis intercept). The point on the y-axis where the semivariance is tending to infinity and no changes are visible is termed sill. The range describes the point of the x-axis (distance) where the difference from sill becomes negligible.

The applied parameters of all semivariograms from delta 2 and delta 1 are shown in Figure 13 and 14. The values to fit the Gaussian functions are shown in Table 2.

**Table 2:** Parameters to describe the semivariogram

	Delta 2014 (North)	Delta 2015 (North)	Delta 2014 (South)	Delta 2015 (South)
Range	480	545	585	610
Sill	3.1	6.0	1.15	1.18
Nugget	0.17	0.08	0.05	0.03

Both datasets from 2014 and both datasets from 2015 have been processed by applying the same mathematical model on the weighted semivariance data. A Gaussian function with fitting parameters Nugget, Sill and Range (Tab. 2) generated the best results. Fitting was chosen graphically. The commented programming script in R to run the interpolation can be found attached.

The interpolation of all four datasets produced rasterized surfaces for each delta in both years with absolute elevation values in a 20 m resolution. The surfaces are shown in Figure 15 and 16. The interpolation of the DGPS data was classified to visualize underlying structures. These intermediate results for both deltas show an obvious decrease in elevation

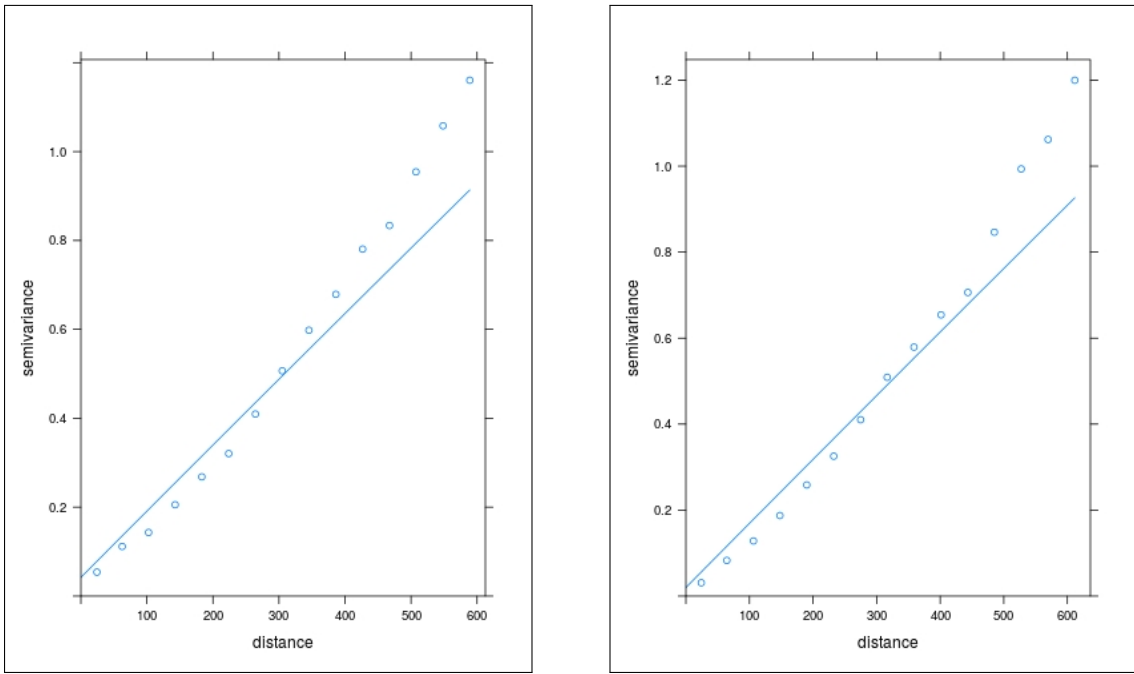


**Figure 14:** Semivariograms of the southern delta from 2014 (left) and 2015 (right)

in distal direction. Both deltas show stripes of same elevation values running roughly parallel the former shoreline of Chaitén town.

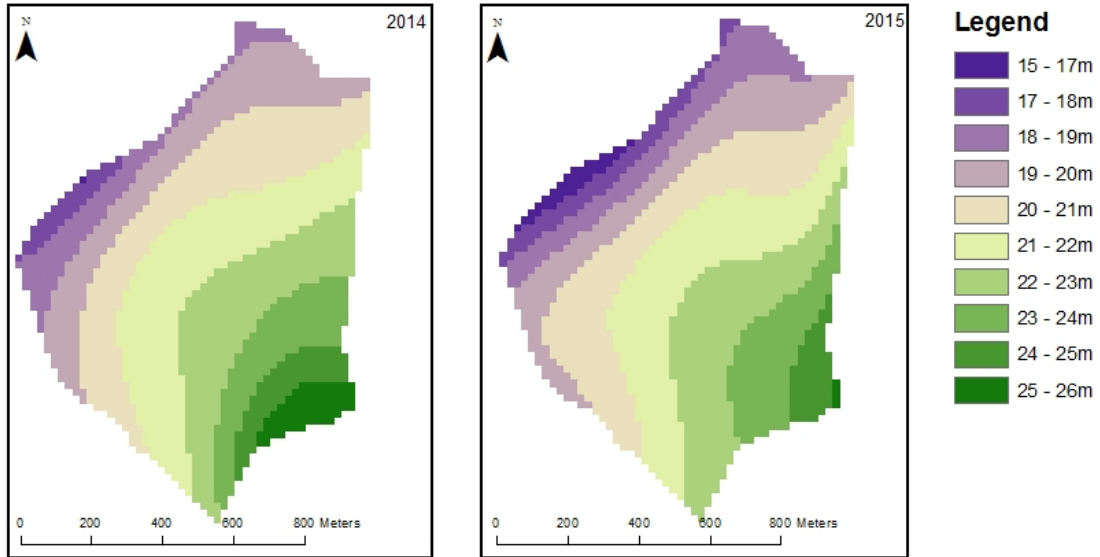


**Figure 15:** Interpolated DGPS data from 2014 and 2015 survey of the northern Chaiten delta

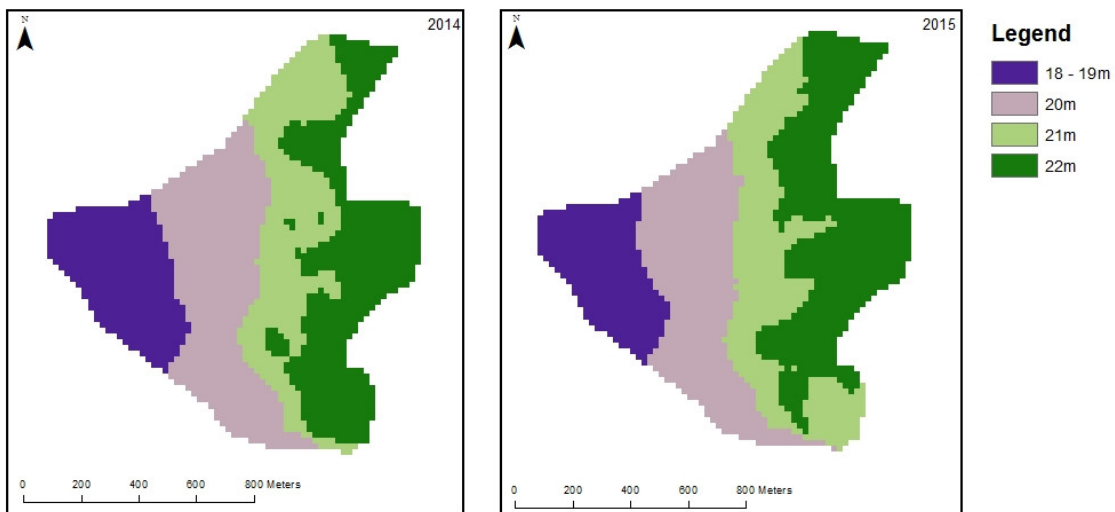


**Figure 16:** Interpolated DGPS data from 2014 and 2015 survey of the southern Chaiten delta

The high values of absolute elevation between 16 m to 25 m for delta 2 and 18 m to 22 m for delta 1 are somehow confusing due to the proximity of the sea level. Mean sea level of Gulf of Corcovado is about 4 m. The discrepancy between the elevation values is a matter of reference heights. The DGPS measurements deliver the height between topography and reference ellipsoid which approximates the earth's surface. The height between topography and geoid is called orthometric height and is approximated by the mean sea level. The geoid height describes the height between reference ellipsoid and geoid and be determined by using a geodetic model (EGM96). The elevation data can be converted by taking this information into account. Nevertheless the absolute elevation values in this study are of secondary interest because analysis is performed by using only the difference values.

### 3.3.2 Volume difference

The volumetric change of the delta between 2014 and 2015 was calculated by subtracting the interpolated elevation rasters. Therefore both rasters had to be intersected by the delta plane because the interpolation produces rectangular maps and both rasters need to have the same amount of cells. A difference of the raster maps detect the changes in elevation for each grid cell between 2014 and 2015. The resulting map contains areas of elevation increase and decrease (change detection). The multiplication of the cell area ( $20 \text{ m} \times 20 \text{ m}$ ) by the summed-up elevation change delivers the total amount of volumetric change. The complete script to run the calculation in R can be found attached.

### 3.3.3 Granulometry

Grain size analysis was done by using the R package *rysgran*. The statistical grain size parameters from sieving results were calculated by using the equations 2,3,4,5 following the method of Folk and Ward (1957). The four parameters of the samples have been determined to find possible spatial trends within the grain size statistics. The focal point

of interest is on the longshore dune samples because they experience the most constant modification by erosional processes due to the location at the delta front. The sediment samples from the delta plane have already been processed after the 2013 survey. The reason for their presence in this study is the potential relationship to the nested samples from 2015 and to have a more comprehensive database to distinguish the different depositional environments.

Results are represented in  $\phi$ -unit to avoid a logarithmic x-axis and make the plots intuitively readable. The  $\phi$  unit can be calculated by using  $\phi = -\log_2(d)$ , where  $d$  is grain diameter in mm.

$$\text{Mean} = \frac{\phi_{16} + \phi_{50} + \phi_{84}}{3} \quad (2)$$

$$\sigma_1(\text{Sorting}) = \frac{\phi_{84} - \phi_{16}}{4} + \frac{\phi_{95} - \phi_5}{6,6} \quad (3)$$

$$\text{Skewness} = \frac{\phi_{16} + \phi_{84} - 2 \cdot \phi_{50}}{2 \cdot (\phi_{84} - \phi_{16})} + \frac{\phi_5 + \phi_{95} - 2 \cdot \phi_{50}}{2 \cdot (\phi_{95} - \phi_5)} \quad (4)$$

$$\text{Kurtosis} = \frac{\phi_{95} - \phi_5}{2,44 \cdot (\phi_{75} - \phi_{25})} \quad (5)$$

The mean describes the average value of sediment sample distribution by considering the average size of the coarsest third, the finest third and the middle third. The sorting parameter measures the grain size variation of samples by encompassing the extreme parts of the distribution. Skewness describes the distribution of the sediment sample in terms of its symmetry. Either a distribution is tending to the coarse grained fraction or to fine grained fraction. The equation of the inclusive graphic skewness follows the method of Folk and Ward (1957) measures both the central part of the distribution and the extremes. Kurtosis describes the ratio of sorting in the central part of a distribution relative to the sorting of the extremes. Hence, the Kurtosis parameter can be considered as a test of normality of a distribution. In Gaussian normal distribution the Kurtosis value is 1. High kurtosis values can be an indication for a sediment sorting due to secondary processes after deposition (Friedman, 1962).

The limits of the statistical parameters (Tab. 3) are based on thousands of sieved sediment samples from various depositional environments. Therefore it is important to bear in mind that the results can vary from the empirical values. Its recommended to interpret the parameters relative to each other and not only absolute values.

**Table 3:** Ranges of  $\phi$  values and associated descriptions by Folk and Ward (1957)

range $\phi$	description		
<i>Sorting</i>			
0.00	-	0.35	very well sorted
0.35	-	0.50	well sorted
0.50	-	0.71	moderately well sorted
0.71	-	1.00	moderately sorted
1.00	-	2.00	poorly sorted
2.00	-	4.00	very poorly sorted
4.00	-	open	extremely poorly sorted
<i>Skewness</i>			
0.30	-	0.10	fine skewed
0.10	-	-0.10	Normal distribution
-0.10	-	-0.30	coarse skewed
-0.30	-	-1.00	strongly coarse skewed
<i>Kurtosis</i>			
0.41	-	0.67	very platykurtic
0.67	-	0.90	platykurtic
0.90	-	1.11	mesokurtic
1.10	-	1.50	leptokurtic
1.50	-	3.00	very leptokurtic

## 4 Results

### 4.1 Chaitén Delta changes between 2014 and 2015

The change detection was done by subtracting ordinary Kriging interpolated DGPS data from 2014 and 2015. The negative values represent elevation increase (m) and positive values elevation decrease (m). The results have been classified in a 0.2 m interval to visualize the different zones of surface variation (Fig. 17).

Figure 17A shows the annual change of delta 2 (enlarged figure attached). The central part of delta 2 decreased in elevation around 0 m – 0.4 m. An elongated narrow higher area orientated from NNW to the center of delta 2 is remarkable. The highest change between 2014 and 2015 can be observed on the longshore dune at the north-western part of the delta. Elevation of this area decreased between 0.8 m and 1.8 m. Also the southern part of the delta shows a vertical decrease of a similar extend. Elevation increase is only noticeable at the western part of delta 2 and shows a risen surface of 0.2 m to 0.6 m. The calculated volumetric change between 2014 and 2015 shows a decrease of  $3,9 \pm 0.9 \cdot 10^5 \text{ m}^3$ .

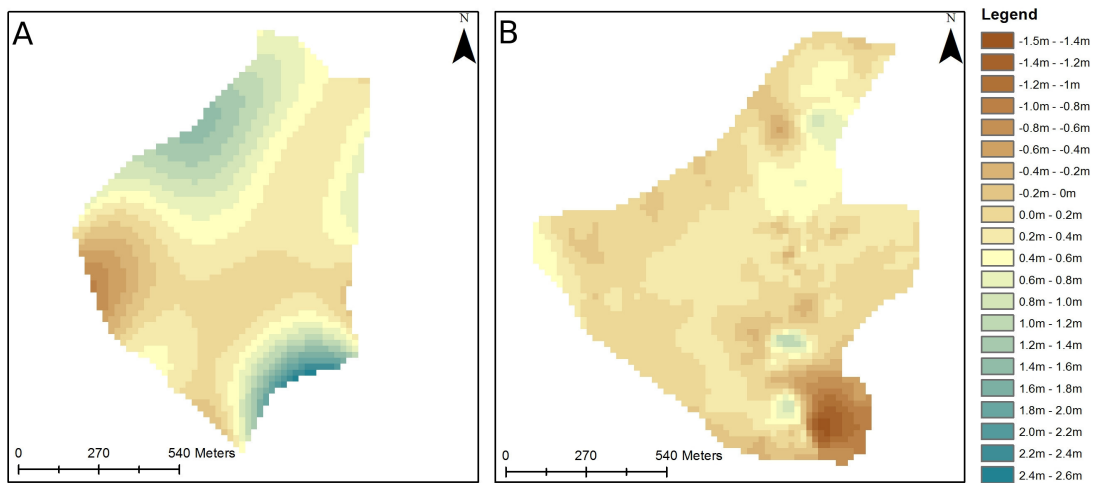


**Figure 17:** Elevation difference of the interpolated DGPS data. Negative values represent elevation increase, positive values elevation decrease in meters.

The changes in delta 1 are much more moderate than in delta 2. Figure 17B shows these changes also in a 0.2 m interval. The most southern peak of the delta shows an elevation increase of 0.6 m to 1.4 m. Two additional but way smaller patches of comparable elevation increase can be observed in the center and the northern part of this delta. These areas are subordinated relative to the complete delta area. The large part of the delta plane shows an decrease between 0.2 m and 0.3 m with some patches of lower decrease around 0.1 m. Some rare patches of higher decrease of around 0.6 m are also noticeable. The volumetric change of delta 1 is about  $1.0 \pm 0.4 \cdot 10^5 \text{ m}^3$ .

An open area of  $1.14 \text{ km}^2$  is located between both deltas (Fig. 8) which could not be measured with the DGPS due to flooding of this area by the river Blanco. The calculated volumes of both deltas have been normalized to determine an averaged volumetric change

for the whole deltaic area of around  $3 \text{ km}^2$ . The systematic vertical error of the DGPS is about 20 mm, this totals in  $0.6 \cdot 10^5 \text{ m}^3$  with respect to the annual volumetric change. The influence of possible interpolation errors (artifacts) was estimated by performing 100 iterative interpolations using 500 randomly sampled DGPS data points. The resulting variance in volume difference was used as the error range to reduce the uncertainties from possible interpolation artefacts.

The complete delta, including the northern part, the southern part and the no-data area changed volumetrically about  $7.8 \pm 2.5 \cdot 10^5 \text{ m}^3$  between 2014 and 2015. From this follows a mean lowering rate of  $257 \pm 80 \text{ mm yr}^{-1}$ .

The absolute volume of the delta can not be determined from the DGPS data without rough assumptions. There is no information about the slope geometry below the sediment body. Hence, a minimum total volume based on the DGPS data and the interpolation was determined to avoid redundant assumptions. The volume above the lowest DGPS point was calculated by subtracting a single value raster (lowest point) of the same spatial extent from the 2015 interpolated surface. This step was done for each grid cell and summed-up to obtain the total minimum volume. The volume for the no-data area between delta 1 and delta 2 has been determined based on the average of the calculated volumes with respect to the complete area. The total minimum volume of the deltaic area amounts  $1.07 \pm 0.1 \cdot 10^7 \text{ m}^3$ .

## 4.2 Sediment characteristics

The results of the 70 sediment samples from 4 different sample locations (Fig. 12) are represented in two bivariate scatter plots (Fig. 18 and 19). Various statistical parameters (Mean, Median, Sorting, Skewness and Kurtosis) have been calculated (Tab. 4, 5, 6 and 7) using well established equations (Folk and Ward, 1957).

The transectional delta samples from 2013 show an averaged mean value of  $0.031\phi$  within a range of  $1.52\phi$  to  $-1.27\phi$ . Sorting values range from  $2.46\phi$  to  $1.28\phi$  with an average of  $1.83\phi$ . This means that the most samples from the delta are dominated by poorly sorted coarse sand. Skewness does not show a direct trend rather it is nearly symmetrical in average. Samples have been taken in four transects (north, northwest, west and southwest) but no direction showed a clear distal/proximal trend in any statistical parameter. Kurtosis of the delta samples ranges between  $1.72\phi$  and  $0.71\phi$  with a mean value of  $1.06\phi$ .

Sixteen samples of four different sub-locations from depositional stream terraces of the Chaiten catchment have been taken in 2015. The mean grain size ranges from  $1.82\phi$  to  $-0.12\phi$  with an average grain size of  $0.9\phi$ . Sorting values are in a wide range from  $2.33\phi$  to  $0.69\phi$  with mean value of  $1.4\phi$ . This implies that some samples are moderately well sorted while others show a very poor sorting factor. Grain sizes are smaller than those from the delta plane and represent medium sand. The distribution of the grain sizes is slightly positive skewed, thus there is an excess of fine material noticeable. No spatial

trend within the four sub-locations could be identified. Kurtosis ranges between  $1.88\phi$  to  $0.7\phi$  with an average of  $1.15\phi$  and therefore shows a leptokurtic distribution.

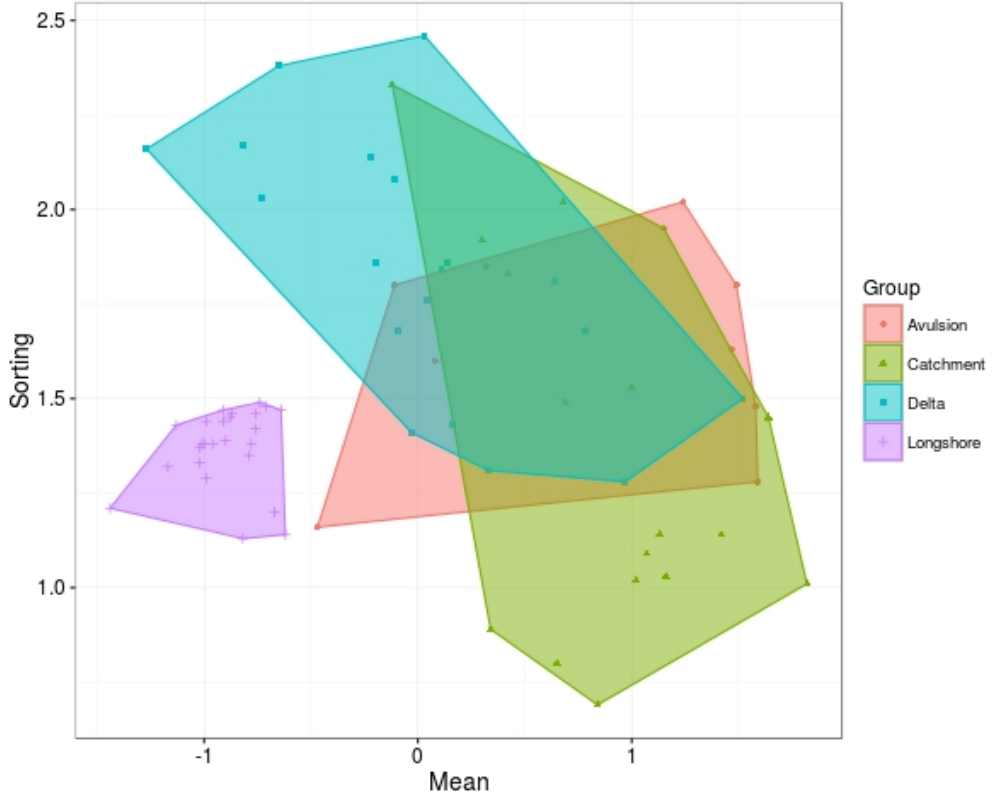


**Figure 18:** Mean and Sorting values of all sediment sampled grouped by origin

The longshore dune which runs from the western peak of the delta in the north-eastern direction is represented in 25 samples of 5 sub-locations. Mean grain sizes range from  $-0.62\phi$  to  $-1.44\phi$  with an average size of  $-0.9\phi$ . Thus, the longshore dune is dominated by very coarse sand although the transectional delta samples are spatially quite close. The sorting of these samples is between  $1.49\phi$  and  $1.13\phi$  with an average of  $1.4\phi$  and therefore still poorly sorted. By averaging the samples to the 5 sub-locations one might interpret a slight trend in sorting to north-eastern direction within the error range. Remarkable are the small ranges of sorting and mean size compared to the other sample locations. Skewness of the longshore samples ranges from  $-0.44\phi$  to  $+0.45\phi$  with a mean value of  $-0.11\phi$ . Kurtosis ranges from  $0.52\phi$  to  $0.81\phi$  with a mean value of  $0.62\phi$ .

The last sample location is the pre-eruption channel near Chaitén town. The sediments have been accumulated before sediment concentration exceeded the transport capacity of the Blanco river and avulsion through the town took place. Mean grain size is between  $1.59\phi$  and  $-0.47\phi$  with an average of  $0.8\phi$ . Sorting of these samples is between  $1.16\phi$  and  $2.02\phi$  with an average of  $1.6\phi$ . Thus, the pre-eruption channel is dominated by poorly sorted coarse sand similar to the delta samples from 2013. Skewness is slightly positive in average like the catchment samples have also shown. Kurtosis ranges between a mesokurtic and leptokurtic distribution with two spikes which show values greater  $1.5\phi$ .

The samples are categorized by the depositional environment using a convex hull to identify differences. The longshore samples show the lowest variance in sorting, mean grain size and kurtosis compared to the rest of the samples. The samples from delta, the pre-eruption channel and the catchment display a common area regarding sorting and mean values but show also different tendencies. The delta samples are tending to a very poor sorting while the catchment samples are slightly better sorted. Skewness and kurtosis from delta and catchment samples are also overlapping but the delta samples are tending to be more negatively skewed and show a higher kurtosis than the catchment samples. However the terrace deposits from the catchment are more positively skewed due to the higher amount of fine grained sediments. The pre-eruption channel shows also a tendency to a more positive skewness but the other parameters are almost completely overlapping the delta and catchment samples.

An alternative display of the data can be found in the attachment (Fig. 31, 32, 33 and 34). All parameters have been plotted as smooth density estimates for each depositional environment. Mean values are marked by dashed lines.

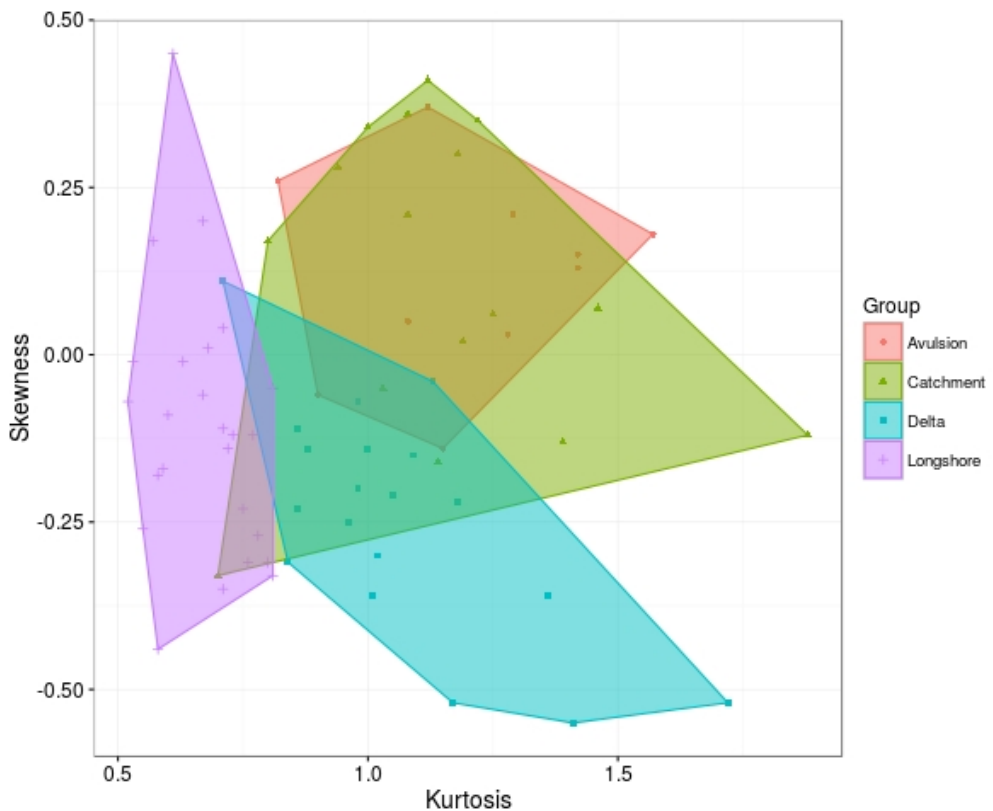


**Figure 19:** Skewness and Kurtosis values of all sediment sampled grouped by origin

Table 4: Results grain size analysis 2013 delta samples

Sample	Mean	Median	Sorting	Skewness	Kurtosis	Description
val01	-1.27	-1.45	2.16	0.11	0.71	Granules, Very poorly sorted, Positive Skewness, Platykurtic
val02	-0.03	0.22	1.41	-0.31	0.84	Very coarse sand, Poorly sorted, Very negative Skewness, Platykurtic
val03	1.52	1.66	1.5	-0.2	0.98	Medium sand, Poorly sorted, Negative Skewness, Mesokurtic
val04	-0.09	0.19	1.68	-0.23	0.86	Very coarse sand, Poorly sorted, Negative Skewness, Platykurtic
val05	-0.82	-0.59	2.17	-0.11	0.86	Very coarse sand, Very poorly sorted, Negative Skewness, Platykurtic
val06	0.14	0.4	1.86	-0.22	1.18	Coarse sand, Poorly sorted, Negative Skewness, Leptokurtic
val07	0.78	1.29	1.68	-0.52	1.72	Coarse sand, Poorly sorted, Very negative Skewness, Very leptokurtic
val08	0.64	1.25	1.81	-0.55	1.41	Coarse sand, Poorly sorted, Very negative Skewness, Leptokurtic
val09	0.33	0.43	1.31	-0.07	0.98	Coarse sand, Poorly sorted, Approx. sym. Skewness, Mesokurtic
val10	-0.73	-0.49	2.03	-0.14	1	Very coarse sand, Very poorly sorted, Negative Skewness, Mesokurtic
val11	0.16	0.4	1.43	-0.14	0.88	Coarse sand, Poorly sorted, Negative Skewness, Platykurtic
val12	-0.2	0.08	1.86	-0.25	0.96	Very coarse sand, Poorly sorted, Negative Skewness, Mesokurtic
val13	0.97	1.29	1.28	-0.36	1.36	Coarse sand, Poorly sorted, Very negative Skewness, Leptokurtic
val15	-0.65	0.01	2.38	-0.3	1.02	Very coarse sand, Very poorly sorted, Very negative, Mesokurtic
n1	0.03	0.7	2.46	-0.36	1.01	Coarse sand, Very poorly sorted, Very negative Skewness, Mesokurtic
nw1	0.04	0.79	1.76	-0.52	1.17	Coarse sand, Poorly sorted, Very negative Skewness, Leptokurtic
w1	-0.11	-0.1	2.08	-0.04	1.13	Very coarse sand, Very poorly sorted, Approx. sym. Skewness, Leptokurtic
sw1	-0.22	-0.1	2.14	-0.15	1.09	Very coarse sand, Very poorly sorted, Negative Skewness, Mesokurtic
start	0.11	0.35	1.84	-0.21	1.05	Coarse sand, Poorly sorted, Negative Skewness, Mesokurtic

Table 5: Results grain size analysis 2013 catchment samples

Sample	Mean	Median	Sorting	Skewness	Kurtosis	Description
Teph03(1)	-0.12	0.15	2.33	-0.05	1.03	Very coarse sand, Very poorly sorted, Approx. sym., Mesokurtic
Teph03(2)	0.68	0.42	2.02	0.17	0.8	Coarse sand, Very poorly sorted, Positive, Platykurtic
Teph03(3)	1	0.57	1.53	0.35	1.22	Medium sand, Poorly sorted, Very positive, Leptokurtic
Teph03(4)	0.3	0.3	1.92	0.02	1.19	Coarse sand, Poorly sorted, Approx. sym., Leptokurtic
Teph03(5)	0.42	0.4	1.83	0.06	1.25	Coarse sand, Poorly sorted, Approx. sym., Leptokurtic
Teph05(1)	1.07	0.82	1.09	0.41	1.12	Medium sand, Poorly sorted, Very positive, Leptokurtic
Teph05(2)	1.42	1.24	1.14	0.28	0.94	Medium sand, Poorly sorted, Positive, Mesokurtic
Teph05(3)	1.13	0.97	1.14	0.3	1.18	Medium sand, Poorly sorted, Positive, Leptokurtic
Teph05(4)	1.82	2.08	1.01	-0.33	0.7	Medium sand, Poorly sorted, Very negative, Platykurtic
Teph05(5)	1.16	1.01	1.03	0.36	1.08	Medium sand, Poorly sorted, Very positive, Mesokurtic
Teph07(1)	0.65	0.57	0.8	0.07	1.46	Coarse sand, Moderately sorted, Approx. sym., Leptokurtic
Teph07(2)	0.84	0.7	0.69	0.34	1	Coarse sand, Moderately well sorted, Very positive, Mesokurtic
Teph07(3)	0.34	0.4	0.89	-0.12	1.88	Coarse sand, Moderately sorted, Negative, Very leptokurtic
Teph09(1)	1.15	1.29	1.95	-0.16	1.14	Medium sand, Poorly sorted, Negative, Leptokurtic
Teph09(2)	1.02	0.86	1.02	0.21	1.08	Medium sand, Poorly sorted, Positive, Mesokurtic
Teph09(3)	1.64	1.68	1.45	-0.13	1.39	Medium sand, Poorly sorted, Negative, Leptokurtic

Table 6: Results grain size analysis 2015 longshore samples

Sample	Mean	Median	Sorting	Skewness	Kurtosis	Description
LS01(1)	-0.64	0.03	1.47	-0.44	0.58	Very coarse sand, Poorly sorted, Very negative, Very platykurtic
LS01(2)	-0.78	-0.44	1.38	-0.23	0.75	Very coarse sand, Poorly sorted, Negative, Platykurtic
LS01(3)	-0.96	-0.76	1.38	-0.09	0.6	Very coarse sand, Poorly sorted, Approx. sym., Very platykurtic
LS01(4)	-0.74	-0.3	1.49	-0.26	0.55	Very coarse sand, Poorly sorted, Negative, Very platykurtic
LS01(5)	-1	-0.89	1.38	-0.01	0.53	Very coarse sand, Poorly sorted, Approx. sym., Very platykurtic
LS02(1)	-0.99	-0.76	1.29	-0.17	0.59	Very coarse sand, Poorly sorted, Negative, Very platykurtic
LS02(2)	-0.62	-0.38	1.14	-0.31	0.76	Very coarse sand, Poorly sorted, Very negative, Platykurtic
LS02(3)	-0.99	-0.86	1.44	0.01	0.68	Very coarse sand, Poorly sorted, Approx. symmetrical, Platykurtic
LS02(4)	-0.67	-0.43	1.2	-0.27	0.78	Very coarse sand, Poorly sorted, Negative, Platykurtic
LS02(5)	-1.02	-0.87	1.33	-0.07	0.52	Granules, Poorly sorted, Approx. sym., Very platykurtic
LS03(1)	-0.88	-0.59	1.45	-0.12	0.73	Very coarse sand, Poorly sorted, Negative, Platykurtic
LS03(2)	-0.87	-0.56	1.46	-0.14	0.72	Very coarse sand, Poorly sorted, Negative, Platykurtic
LS03(3)	-0.82	-0.73	1.13	-0.12	0.77	Very coarse sand, Poorly sorted, Negative, Platykurtic
LS03(4)	-0.91	-0.68	1.47	-0.06	0.67	Very coarse sand, Poorly sorted, Approx. sym., Platykurtic
LS03(5)	-0.91	-0.63	1.44	-0.11	0.71	Very coarse sand, Poorly sorted, Negative, Platykurtic
LS04(1)	-0.76	-0.24	1.42	-0.35	0.71	Very coarse sand, Poorly sorted, Very negative, Platykurtic
LS04(2)	-0.71	-0.15	1.48	-0.33	0.81	Very coarse sand, Poorly sorted, Very negative, Platykurtic
LS04(3)	-0.9	-0.6	1.39	-0.18	0.58	Very coarse sand, Poorly sorted, Negative, Very platykurtic
LS04(4)	-1.02	-0.91	1.37	-0.01	0.63	Granules, Poorly sorted, Approx. sym., Very platykurtic
LS04(5)	-0.76	-0.24	1.46	-0.31	0.8	Very coarse sand, Poorly sorted, Very negative, Platykurtic
LS05(1)	-1.13	-1.21	1.43	0.2	0.67	Granules, Poorly sorted, Positive, Platykurtic
LS05(2)	-1.17	-1.28	1.32	0.17	0.57	Granules, Poorly sorted, Positive, Very platykurtic
LS05(3)	-0.79	-0.65	1.35	-0.05	0.81	Very coarse sand, Poorly sorted, Approx. symmetrical, Platykurtic
LS05(4)	-1.01	-0.94	1.38	0.04	0.71	Granules, Poorly sorted, Approx. sym., Platykurtic
LS05(5)	-1.44	-1.81	1.21	0.45	0.61	Granules, Poorly sorted, Very positive, Very platykurtic

Table 7: Results grain size analysis 2014 pre-eruption channel samples

Sample	Mean	Median	Sorting	Skewness	Kurtosis	Description
AV01	0.32	0.41	1.85	0.05	1.08	Coarse sand, Poorly sorted, Approx. symmetrical, Mesokurtic
AV02	0.08	-0.2	1.6	0.37	1.12	Coarse sand, Poorly sorted, Very positive, Leptokurtic
AV03	1.59	1.54	1.28	0.15	1.42	Medium sand, Poorly sorted, Positive, Leptokurtic
AV04	1.47	1.5	1.63	0.03	1.28	Medium sand, Poorly sorted, Approx. symmetrical, Leptokurtic
AV05	1.49	1.42	1.8	0.18	1.57	Medium sand, Poorly sorted, Positive, Very leptokurtic
AV06	-0.47	-0.55	1.16	0.21	1.29	Very coarse sand, Poorly sorted, Positive, Leptokurtic
AV07	-0.11	-0.48	1.8	0.26	0.82	Very coarse sand, Poorly sorted, Positive, Platykurtic
AV08	1.58	1.7	1.48	-0.14	1.15	Medium sand, Poorly sorted, Negative, Leptokurtic
AV09	0.69	0.65	1.49	0.13	1.42	Coarse sand, Poorly sorted, Positive, Leptokurtic
AV10	1.24	1.47	2.02	-0.06	0.9	Medium sand, Very poorly sorted, Approx. symmetrical, Platykurtic

### 4.3 Sediment Budget

Estimating a simplified sediment budget for the distribution of volcaniclastic sediments requires the minimum amount of sediment deposited in the catchment by the volcanic eruption (input) and the minimum amount of sediment which left the drainage basin (output). The delta area was defined as the output parameter because setting up a sediment budget requires spatial boundaries. Grain size distributions of the delta and the catchment samples suggests that a certain amount of the transported sediment was not deposited on the delta but rather was transported directly into the ocean basin of the Gulf of Corcovado. Samples from the catchment are characterized by smaller grain sizes and a more positive skewness than delta plane samples show. Therefore it will be assumed that the lack of fine sediment fractions within the delta was already eroded or rather never accumulated. The total volumetric inflow of the lahars through the delta reservoir can be estimated following the method of (Lavigne and Thouret, 2003).

$$C_m = V_s \cdot (1 - e) \cdot \frac{100}{R} \quad (6)$$

Where  $C_m$  is the mean sediment concentration by volume (%),  $e$  the voids ratio and  $R$  the total inflow in  $\text{m}^3$ . Rearranging the equation to  $R$  gives:

$$R = -\frac{100 \cdot (e - 1) \cdot V_s}{C_m} \quad (7)$$

The void ratio is a parameter which is related to the volume of pore-space ( $V_V$ ) and the volume of solids ( $V_S$ ) and therefore can be calculated by using the porosity  $\phi_S$  of the sediments.

$$e = \frac{V_V}{V_S} = \frac{\phi_S}{1 - \phi_S} \quad (8)$$

Using the equations above means to make assumptions for the parameters  $C_m$  and  $\phi_S$ . A range for the sediment concentration in lahars of 20-50% was given by several authors (e.g. (Lavigne and Thouret, 2003; Pierson, 2005; Vallance and Iverson, 2015)) and represents the rheological type of a hyperconcentrated flow. The porosity was estimated in a range of 30-45% and seemed realistic comparing to the values of (Ferrucci et al., 2005). The upper threshold could be slightly higher but decision came due to the poor sorting values of the sediment samples (Rogers and Head, 1961). The total inflow has been calculated using equations 8 and 7 for various possibilities within the assumption ranges (see discussion). The total inflow results  $1.7 \pm 1.3 \cdot 10^7 \text{ m}^3$ . Subtracting the minimum amount of sediment deposited at the shoreline (Chaitén delta) from the total inflow gives the volumetric amount of sediment delivered to the ocean basin.

Figure 20 shows a simplified sketch of the sediment budget. A sediment storage within the catchment of at least  $0.3 \pm 1.3 \cdot 10^5 \text{ m}^3$  was estimated using the minimum erupted tephra volume which entered the Chaitén catchment of  $2 \cdot 10^7 \text{ m}^3$  (Pierson et al., 2013; Alfano et al., 2011) and the calculated output values from the DGPS data of  $1.7 \pm 1.3 \cdot 10^7 \text{ m}^3$ .

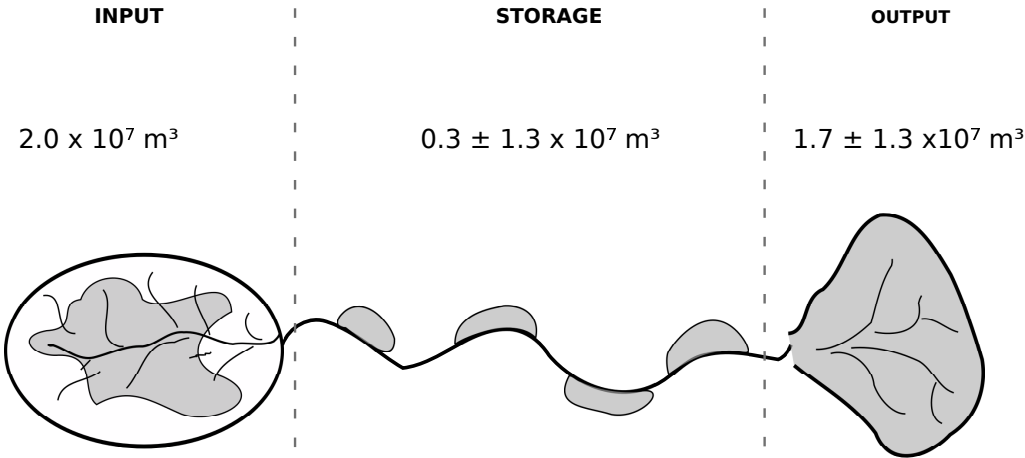


**Figure 20:** Subdivisions of river systems in terms of erosion, transfer/storage and sedimentation and the conceptional sediment budget after (Hinderer, 2012)

Table 8 shows the main physical parameters of the sedimentary response and deposits. The volcaniclastic sediments consist basically of two types; the lithic fraction (type A: densities of  $1760 - 2490 \text{ kg m}^{-3}$ ) and the pumicous fraction (type B: densities of  $1300 - 1600 \text{ kg m}^{-3}$ ) (Pierson et al., 2013). The bulk density range was calculated by considering the percentage of the particular occurrence of the sediment type fractions. Sediment masses and errors are based on this density ranges.

**Table 8:** Main physical parameters of the sediment deposits and the catchment following the eruption of Chaitén volcano.

was	symbol	value	unit	source
drainage area	A	77	$\text{km}^2$	Pierson et al. (2013)
sediment density (type A)	$\rho_A$	$1760 - 2490$	$\text{kg m}^{-3}$	Pierson et al. (2013)
sediment density (type B)	$\rho_B$	$1300 - 1600$	$\text{kg m}^{-3}$	Pierson et al. (2013)
sediment (bulk) <sup>1</sup> density	$\rho_{\text{bulk}}$	$1970 \pm 120$	$\text{kg m}^{-3}$	after Pierson et al. (2013)
Porosity	$\phi_{\text{bulk}}$	30 – 45	%	after Ferrucci et al. (2005)
time since eruption	t	8	yr	
total erupted volume (2008 - 2009)	$V_t$	$0.5 - 1.0 \cdot 10^9$	$\text{m}^3$	Alfano et al. (2011)
min. volume (in Chaitén catchment) <sup>2</sup>	$V_{c_{\min}}$	$2.0 \cdot 10^7$	$\text{m}^3$	Pierson et al. (2013)
min. delta volume	$V_d$	$1.07 \pm 0.1 \cdot 10^7$	$\text{m}^3$	DGPS data
min. delta mass	$M_d$	$2.1 \pm 0.5 \cdot 10^7$	t	DGPS + density
annual sediment loss (vol.)	$\Delta V_d$	$7.8 \pm 2.5 \cdot 10^5$	$\text{m}^3$	DGPS
annual sediment loss (mass)	$\Delta M_d$	$1.53 \pm 0.6 \cdot 10^6$	t	DGPS + density
area delta (reservoir area)	$A_{\Delta\text{elta}}$	3	$\text{km}^2$	Google Satellite Image (2016)
lowering rate <sup>3</sup>	L	$257 \pm 80$	$\text{mm yr}^{-1}$	DGPS

<sup>1</sup>) Bulk density results from 60-95% of lithic sediment (type A) and 5-40% pumicous sediment (type B).

<sup>2</sup>) Alfano et al. (2011) estimated the total erupted volume of the 2008-2009 eruption on  $0.5 - 1.0 \text{ km}^3$ . Based on Alfano's isopache map Pierson et al. (2013) derived a minimum tephra volume of  $2.0 \cdot 10^7 \text{ m}^3$  deposited within the Chaitén catchment.

## 5 Discussion

### DGPS data

The 2008-2009 eruptive phase of the Chaitén volcano caused rapid channel bed aggregation and channel switching due to extreme volcaniclastic sediment input to the river system. The lowermost part of the river avulsed and a  $3 \cdot 10^6 \text{ m}^2$  deltaic area formed by hyperconcentrated flows. Based on the two DGPS surveys in 2014 and 2015 it was possible to quantify the annual change of the sediment body of  $7.8 \pm 2.5 \cdot 10^5 \text{ m}^3$ .

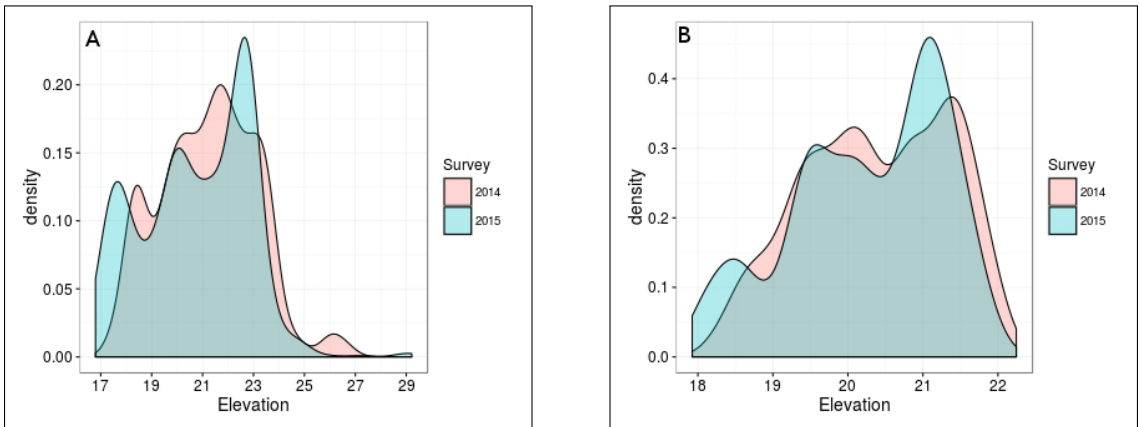


**Figure 21:** Density plots of the DGPS data from delta 2 (A) and delta 1 (B)

The distribution of the DGPS data shows a multimodal distribution in both years. Figure 21 shows a smooth density estimate based on the DGPS data. The y-axis shows the frequency divided by the number of measurements (density) and the x-axis shows the classes of measurements (elevation). Density plots provide similar information as histograms but they show a continuous distribution of the data rather than stick to fixed classes.

Reasons for multimodal distributions could be the presence of extraordinary extreme values or that the DGPS data represents only a subset from the total elevation distribution of the delta. Both reasons are unlikely because the transectional paths of the measurements avoid major lacks of data and extreme values would be noticeable in the density plots (Fig. 21). Natural processes are often following normal distributions. The multimodal distribution could be the result of additive surface forming processes. If e.g. the underlying distribution of the surface morphology, formed by wave and tide erosion, is following a Gaussian function and sheet and/or rill erosion would also follow a Gaussian distribution than the combination of these processes could be represented in a multimodal distribution. Both datasets from 2014 and 2015 have been spatially interpolated using the geostatistical method, ordinary Kriging. Spatial interpolation predicts values in a raster cell from a limited number of data points within the range of these measured points. Using spatial interpolations implicates the assumption that spatially distributed objects (in this case elevation values) are spatially correlated. Using the ordinary Kriging method considers distance and degree of variation between the known data points. Deterministic methods

(e.g. Inverse Distance Weighting, Nearest Neighbour, Spline) calculate values for each grid cell by examining surrounding data points within a certain radius. Ordinary Kriging and IDW have been applied on the DGPS data to evaluate the quality of the interpolation. The IDW method delivered slightly higher results but within the same order of magnitude than ordinary Kriging. Ordinary Kriging method was chosen because the longshore dune at the western part of the delta was represented in contrast to IDW. Interpolating data implicates always to increase the quantity of the data but also to degrade the quality of the measured data by take the complete dataset into account.

The interpolation of the DGPS data produced a rectangular surface and ordinary Kriging method automatically extrapolated regions outside of the delta plane but within the spatial range. Therefore the interpolated raster surfaces have been cropped by a polygon shapefile derived from Google Earth Satellite Image to obtain the same amount of raster cells within real delta area. A disadvantage of this method are the rough cuts at the boundary and depicts a potential error source. Subtracting two raster datasets with a defined cell size of 20 m x 20 m delivers the elevation differences between both surfaces (script attached). Evaluating weather the data contains influencing artefacts or significant errors from the interpolation was done by a sensitivity test. Therefore the volume difference calculation was performed with a sample size interval of 10 to examine the consistence of the data (Fig 22 and 23).

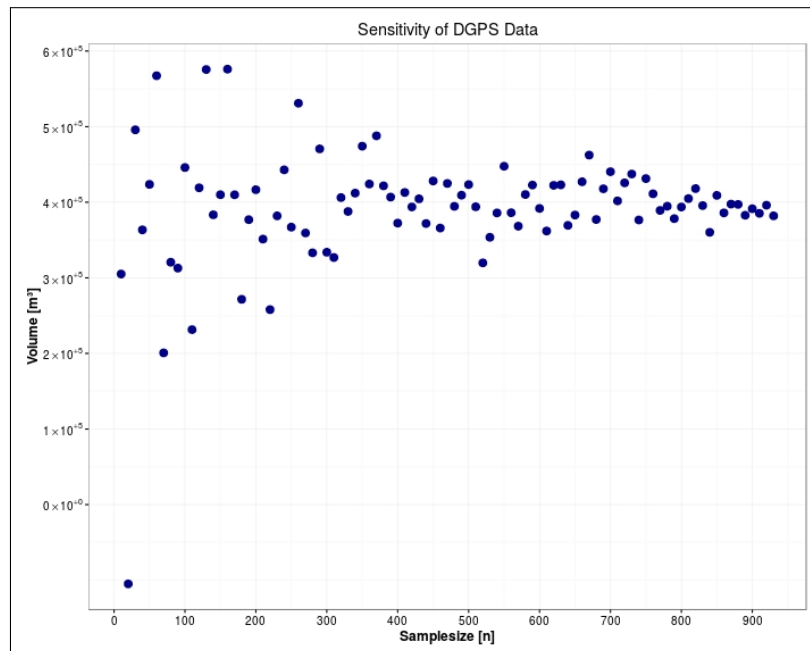


**Figure 22:** Volume difference calculation of the northern delta (delta 2) in a successive sample size interval ( $n=10$ )

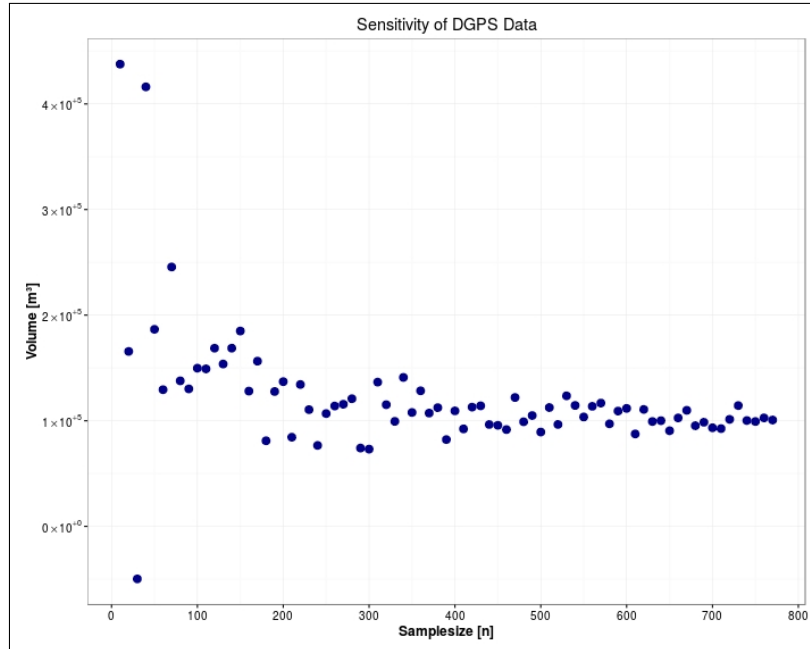


**Figure 23:** Volume difference calculation of the southern delta (delta 1) in a successive sample size interval ( $n=10$ )

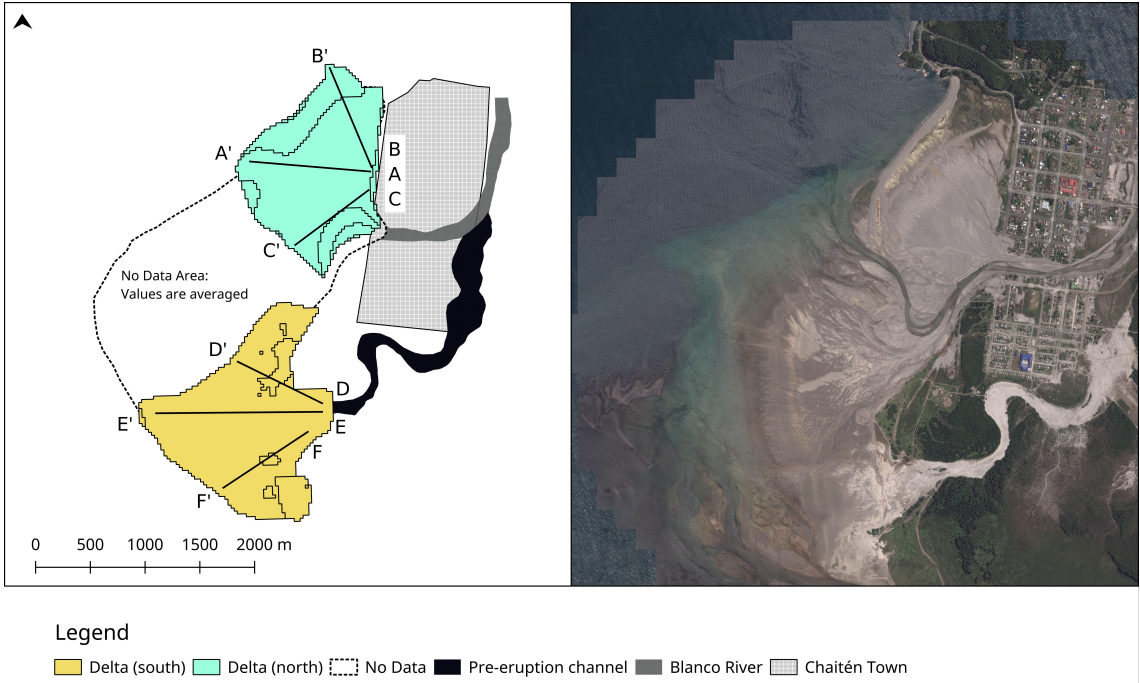
Sampling was done by following a uniform distribution to avoid spatially clustered samples to calculate the volume. The figure shows a decrease in variance with increasing sample size and final at  $3.9 \cdot 10^5$  m<sup>3</sup> for the delta 2 (Fig. 22). The values between 500 and 1000 data points already average at the finally resulting volumetric change. This calculation examines the sensitivity of the data regarding the sample size and shows that the data does not contain significant artifacts which manipulate the volume determination. Figure 23 shows the same test applied on delta 1 using a sample size range from 10 to 770 with an interval of 10. The southern delta shows even better results and confirms the reliability of the DGPS data. Volume calculation final at  $1.0 \cdot 10^5$  m<sup>3</sup>.

The results of the volume difference (Fig. 17), show several patches of elevation decrease and elevation increase of both deltas. A quantification of the different processes that are modifying the surface of the delta is not possible based on the DGPS data. Nevertheless the longshore dune and the southern part of delta 2 can be allocated to erosional processes because grain size analysis shows better sorting and a negative skewness. Only one region of delta 2 shows considerable high elevation increase (Fig. 17A) at the western end. The Google Satellite Image from 2016 (Fig. 24), shows the course of the river Blanco at the channel mouth. Elevation increase of this part was interpreted as sedimentation of suspended sediment load from the river. The northern and southern part show expected high values of elevation decrease at the longshore dune and undercut slope of river Blanco. The longshore dune of the delta is continuously eroded and modified by wave and tidal erosion as confirmed by field observations and grain size analysis. The southern part is located directly at an undercut slope of the Blanco river and therefore highly influenced by fluvial erosion. The central part decreased up to 40 cm and could represent different additive

processes (compaction-driven subsidence, erosion and flattening). The southern delta shows several small points of elevation increase. These points are probably interpolation errors, called bull eyes. Size and shape of these small locations are typical for the bull's eye effect (Luo et al., 2008). The most southern part displays a larger region of elevation increase and shows sediment input of the Negro river from the adjacent catchment. The main part of delta 1 decreased in elevation around 0 – 40cm and could represent beside erosional processes also compaction-driven subsidence.

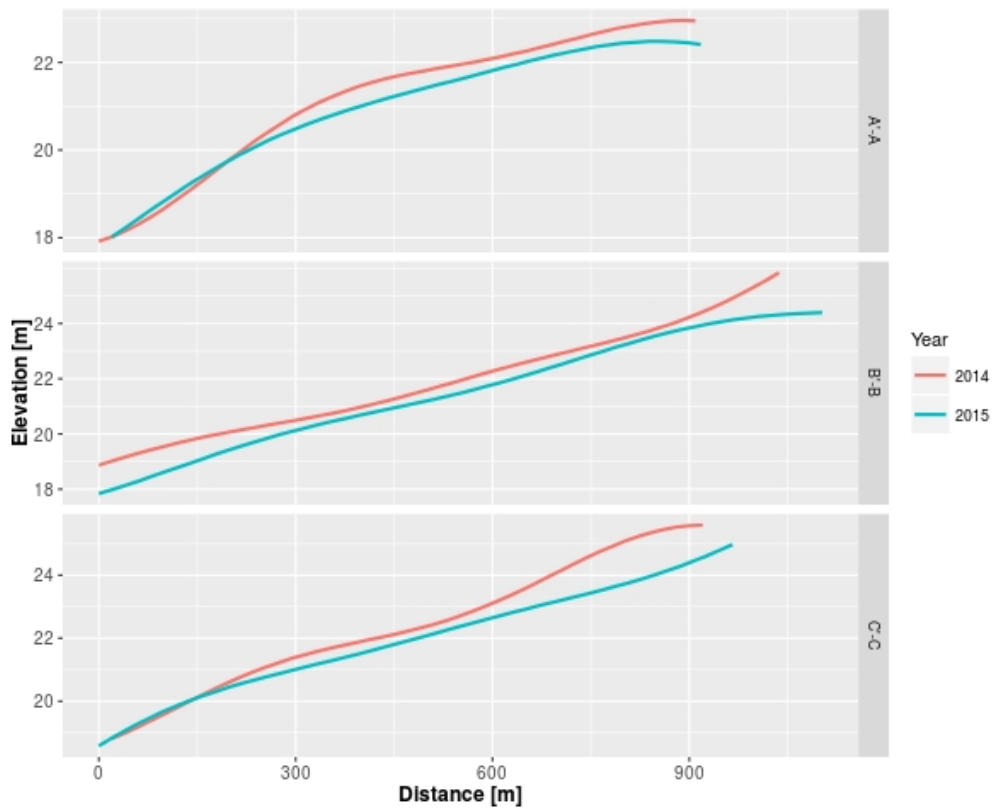
A typical parameter to characterize deltas are subsidence rates because all deltas are sinking and flattening over time. Subsidence describes only the reduction of a surface relative to a reference level (e.g. mean sea level, reference ellipsoid, geoid shape) but does not define the underlying process which led to the surface reduction. Hence, general subsidence rates are suitable to describe the development of a delta but not for comparison, especially if the origin of subsidence is not known. The complete deltaic area of Chaitén shows an averaged lowering rate of  $258 \pm 80 \text{ mm yr}^{-1}$  based on the DGPS data. The averaged lowering rate without the regions that were allocated as erosional processes (longshore dune, fluvial sedimentation/erosion) and therefore could be compaction-driven, results still in  $200 \text{ mm yr}^{-1}$ . Subsidence rates of this magnitude of order are only known from compaction due to ground water pumping (Higgins et al., 2013; Erban et al., 2014) or from porosity reduction due to earthquakes (Wang et al., 2001). Whelley et al. (2011) found evidence for subsidence rates of unconsolidated pyroclastic flow deposits of  $10 \text{ mm yr}^{-1}$  within the first three years after the eruption of the Lascar volcano in Chile. It is unlikely that the lithostatic pressure from the overlying pumice-rich sediments (averaged min. 3 m thickness) can overcome the pore water pressure to reduce porosity suchlike that the surface sinks up to 400 mm. On the contrary, the morphology of the interpolated DGPS data shows a fairly smooth and constant sinking surface.

Figure 24 shows an overview map with profile transects. The comparison of a profile along the delta from 2014 and 2015 superiorly visualizes the morphology and changes of the deltas' surface than raster maps do.



**Figure 24:** Schematic drawing of the Chaitén depositional setting with profile transects and a Google Satellite Image (2016) of the same scale and orientation

Profile A shows the main decrease of the surface in the central and proximal part of the delta (Fig. 25). The distal part shows a slightly increase of the surface which is probably the result of sedimentation of the suspended load from the river. The morphology of this segment shows a flattening and smoothing of the surface from 2014 to 2015. Profile B decreased in the distal and proximal part up to 1.6 m. The central part shows a fairly continuous decrease. Profile C is characterised by high decline in the proximal section and decreased moderately in the central part. The distal part does not show any variation, which could also be the result of current sedimentation. The morphology is also flattening. Profile D from delta 1 shows a clear flattening of the surface. The asperity of the 2014 profile could either be an interpolation error or a temporary formed incision channel perpendicular to the transect. Profile E changed a lot in the most distal part and continuously in central part. The spiky asperities are interpreted as interpolation errors. The profile F shows rather the effect of bull eyes than the real slope of the delta (Fig. 17).



**Figure 25:** Vertical exaggerated elevation profiles of the northern delta.

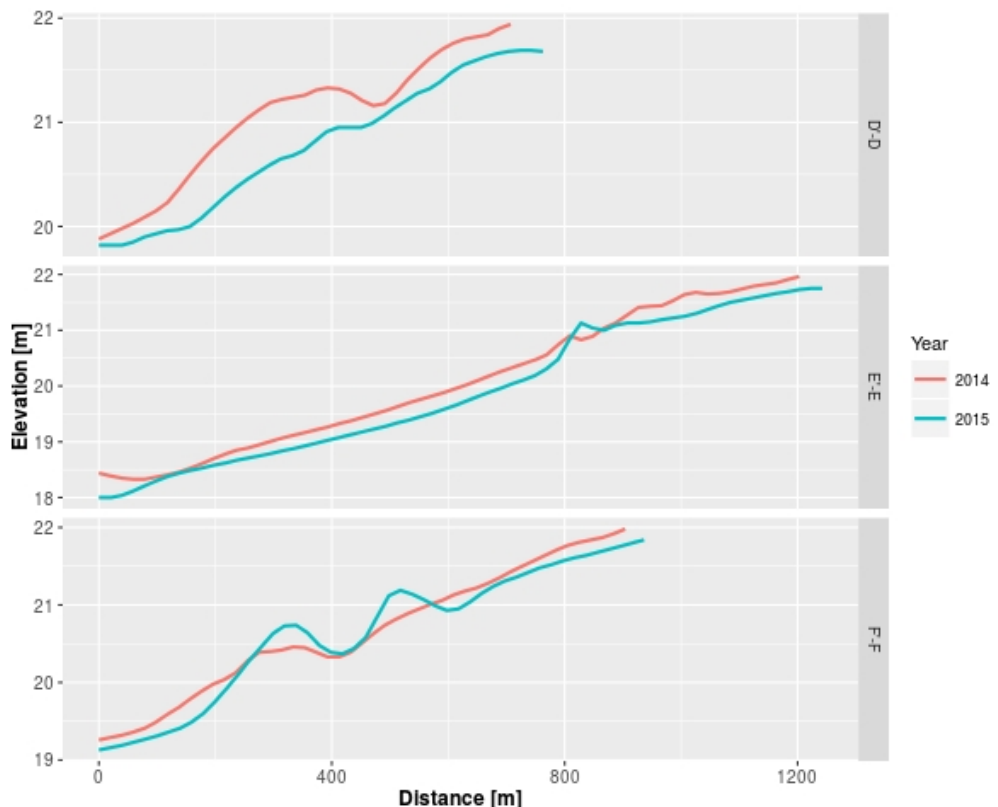


**Figure 26:** Vertical exaggerated elevation profiles of the southern delta.

## Sediment characteristics

Grain size analysis is an often used method to reconstruct the sedimentological processes which caused the deposition of sediments. The transportation processes of the volcaniclastic deposits are already known and have been described by Pierson et al. (2013). The objective of the grain size analysis of this study is to identify the current modifying and therefore erosional processes on four different depositional environments. Figure 11 shows the sample locations of the longshore dune, the pre-eruption channel, the delta plane and the deposits from upstream the catchment. Grain size analysis of volcaniclastic sediments is a common method in volcanic geomorphology but rarely discussed.

Processes or depositional environments of quartz-based sediments are usually deviated from statistical parameters like mean, sorting, skewness and kurtosis. The underlying fact which allows this possibility is the relation of grain size and energy. Water with high energy (e.g. in steep mountain rivers) can transport both bed load (sand and gravel) and suspended load (clay and silt). The amount of transported sediment decreases with decreasing energy of the water. Suspended load settles from the water column and bed load cannot transported anymore. Beach sands are changing their sorting parameter after the deposition due to wave and tidal energy. The oscillation of the water leads to better sorting due to the forward and backward movement of the grains. Furthermore longshore drift causes fine spatial gradients in grain size along the coast.

Volcaniclastic sediments are often characterized by the occurrence of pumice. Pumice is a common product of explosive volcanism, it is a highly unusual geologic material, consisting of very vesicular silicic to mafic glass foam (Fisher and Schmincke, 2012). Densities of dry pumice range between  $0.4 \text{ g cm}^{-3}$  and  $1.3 \text{ g cm}^{-3}$  and thus have different hydrological behavior than a quartz grain of  $2.6 \text{ g cm}^{-3}$ . Pumice is only one part of the volcaniclastic bulk composition but other products like obsidian, rhyolite or wall rock show more comparable density values regarding their hydrological behavior. Manville et al. (1998) have shown that small pumice grains are faster water-saturated than bigger grains and sink faster. The density of water-saturated pumice increases up to  $1.6 \text{ g cm}^{-3}$  and shows a similar hydrological behavior to other grains. Nevertheless, pumice grains in the coarse sand fraction do not necessarily represent the depositional environment or the transporting process and can be easily misinterpreted. Deposits of volcaniclastics can have a coarsening grading trend with distance or an inverse grading within a lacustrine facies.

The eruption of the Chaitén volcano mantled flanks and hillslopes and caused hyperconcentrated flows through the erosion of them. Sedimentation started when the accommodation space could not compensate the high sediment concentration of the stream anymore and took place in the southern delta. Then the pre-eruption channel plugged and the river avulsed through Chaitén town and formed the northern delta. Wave and tide activity modified the delta front and formed the longshore dune.

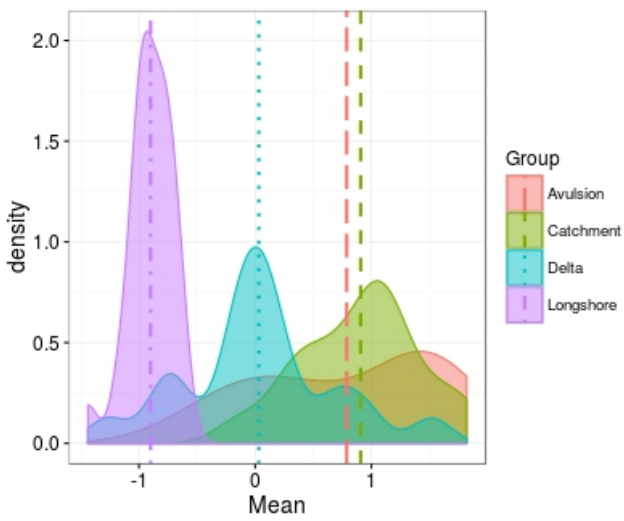


**Figure 27:** Density plots of the sediment samples from different depositional environments

The density plot (Fig.27) shows the mean values of all samples grouped by the depositional environment. The longshore samples in general are poor in fines because wave and tide activity already eroded this fractions. The sample values are quite close to the mean and are poorly sorted. The delta samples are smaller than the longshore samples but greater than the samples from pre-eruption channel and the catchment. Hence, a coarsening trend with distance is noticeable. A further fining of the averaged mean can be identified

first in the pre-eruption channel and then in the catchment. All samples, except the catchment samples, have been taken from the surface exposed to the atmosphere. It is an open question how these samples are clearly representing the deposition process because the surface has been modified by rain, channel incision, wind and the anthropogenic impact. The most reliable samples are the longshore samples because 1) the method of sampling reduces the potential of errors and 2) wave and tide erosion began directly after the deposition and reworked the deposits continuously till now. The catchment samples have been taken from a layer of the lahar deposits and represent a less influenced sediment composition than the rest of the samples. It is likely that the amount of fines within the catchment samples have also been a part of the other samples before erosion of the deposits took place. Density plots of the parameters mean, sorting, skewness and kurtosis can be found attached. The sorting values of all samples are spread over a wide range. Only the longshore samples, which are still poorly sorted, do not scatter as much as the rest and therefore are more reliable. Modification of the grain size distributions by tidal energy and waves could cause the relative better sorting. Furthermore the delta and longshore samples are negatively skewed. This means that there is an excess of coarse grains and a lack in fines. Both the ongoing erosion and the discharge during the deposition generated the negative skewness. The samples from catchment and the pre-eruption channel are more positively skewed and represent a more initial composition of the sediments. The kurtosis values of the samples from catchment, pre-eruption channel and the delta are averaging around 1 even though they are widely spread. Only the longshore samples show a lower value. Friedman (1962) suggests that low and high values in kurtosis imply that the sorting of the sediments was partly generated in a high-energy environment (Rajganapathi et al., 2012) like the coast of Chaitén. Grain size statistics suggests that 1) a certain amount of sediments never was deposited at the shoreline but rather got directly transported into the

ocean basin and 2) tides and waves are highly modifying the longshore dune.

### Sediment Budget

The underlying principle of a sediment budget is the mass conservation of matter. Slaymaker (2003) defined a sediment budget as the accounting of sources, sinks, and redistribution of sediments in an unit region over an unit time. It is important to define the focus of a study before setting up a sediment budget. In most cases it is not possible to apply a complete mass balance because also biochemical fluxes of nutrients and solutes are part of the budget (Hinderer, 2012). This study tries to apply a simplified sediment budget of the erupted volcaniclastic sediments following the 2008-2009 Chaitén eruption. Therefore the watershed is defined as the unit region and the time is given through the date of the eruption. To solve equation 6, the output parameter was equated with the estimated total inflow of the lahars. Estimations from (Pierson et al., 2013) of the minimum total erupted volume of  $2.0 \cdot 10^7 \text{ m}^3$  which were accumulated within the Chaitén catchment was used as the input parameter. This parameter does not have any error range and is not very reliable. The input estimation is based on the isopach map from Alfano et al. (2011). A minimum volume of  $1.07 \cdot 10^7 \text{ m}^3$  of the delta was obtained by subtracting the deltas surface from 2015 from a single value raster of lowest elevation point. A systematic error of 20 mm from the DGPS equipment totals in  $0.1 \cdot 10^6 \text{ m}^3$  with respect to the deltas area of  $3 \cdot 10^6 \text{ m}^2$ .

Quantifying the sediment loss which was transported into the ocean basin is not possible without assumptions. The usual way to determine the amount of sediments which already left a reservoir, is to calculate the trapping efficiency. The trapping efficiency is the proportion of incoming sediment that is deposited, or trapped, in a reservoir pond (Verstraeten and Poesen, 2000). Various equations exist to calculate the trapping efficiency for all types of reservoirs. Each model differs greatly in terms of their complexity, inputs and requirements (Jothiprakash and Garg, 2008). The only models to calculate the trapping efficiency of the Chaitén delta reservoir include the settling velocity and the discharge of the Blanco river. The limited parameters from the DGPS and grain size data exclude several techniques. The discharge of the delta-forming hyperconcentrated flows could be estimated by making assumptions based on literature but the settling velocity of grain sizes within a range of  $-1.5 - 1.5\phi$  is not possible to determine. The bulk density of such mass flows would not allow a single grain to settle down from the sediment-water mixture. Stoke's law cannot be applied on density currents.

Lavigne and Thouret (2003) calculated the mean sediment concentration of rain-triggered lahars at the Merapi Volcano by using equation 7. By making assumptions about the mean sediment concentration and the void ratio it is possible to solve the equation for the total inflow. The mean sediment concentration for hyperconcentrated flows ranges between 20% and 60% (Lavigne and Thouret, 2003; Pierson, 2005). The effective porosity of unconsolidated volcaniclastic sediments was set to 30% - 45% (Ferrucci et al., 2005). The total inflow was calculated for all possible values within the mentioned ranges with

an interval of 5% for the sediment concentration and 0.5% for the porosity. The results are averaging at  $1.7 \cdot 10^7 \text{ m}^3$  (Fig. 28). The minimum calculated total inflow volume is about  $3.2 \cdot 10^6 \text{ m}^3$  and the maximum value about  $3 \cdot 10^7 \text{ m}^3$ . The stored volume within the catchment was estimated by using the minimum tephra input from Pierson et al. (2013) of  $2 \cdot 10^7 \text{ m}^3$  and the total inflow of  $1.7 \pm 1.3 \cdot 10^7 \text{ m}^3$  following the method of Lavigne and Thouret (2003).

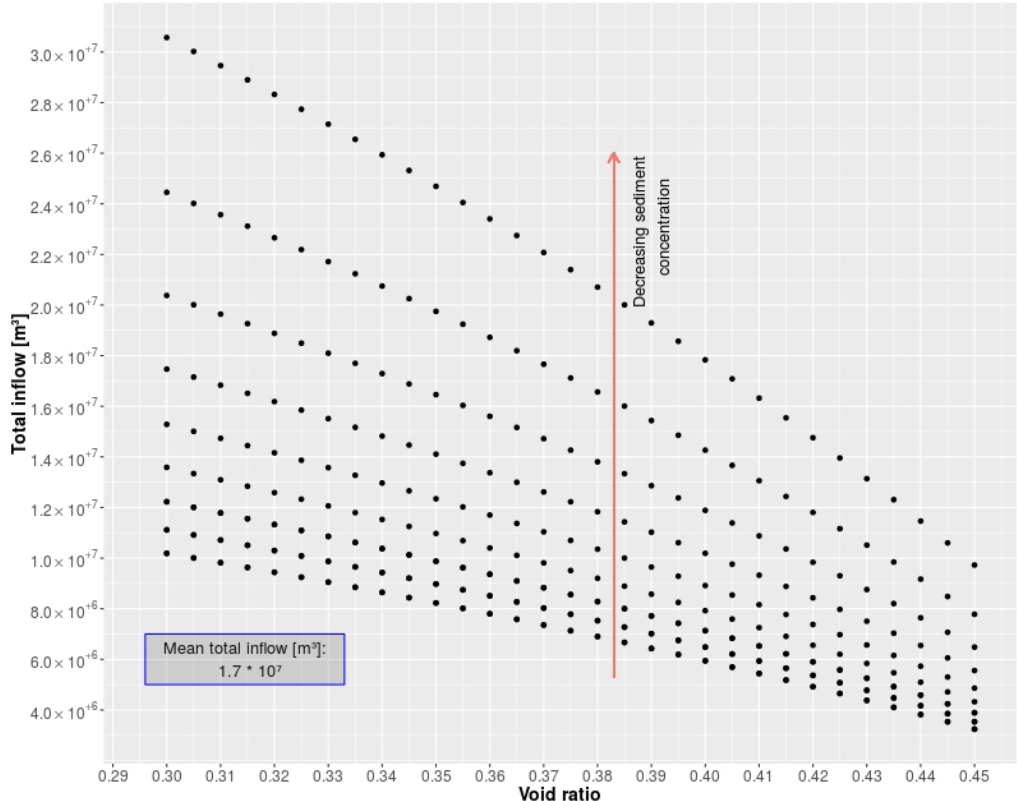


**Figure 28:** Calculation of total inflow volume for different porosity and sediment concentration values

Constructing the sediment budget provides several problems due to incomplete information from literature and rough assumption regarding the total inflow. The average values seem to fit perfectly but the high error ranges generates conflictive interpretations. The mean sediment output of  $1.7 \cdot 10^7 \text{ m}^3$  produces a mean sediment storage of  $0.3 \cdot 10^7 \text{ m}^3$  by using the input estimation of Pierson et al. (2013). A sediment storage of  $1.6 \cdot 10^7 \text{ m}^3$  can be calculated by using the lower boundary of the error range from the output parameter. This means that almost the same amount of sediment which already has been mobilized is still stored within the catchment. The upper boundary of the error range would cause a negative storage of  $-1 \cdot 10^7 \text{ m}^3$  which is not possible for an ideal mass balance but also conceivable. It was thought that the last eruption before 2008 occurred 5000 years ago. Lara et al. (2013) found evidence for an eruptive activity of Chaitén volcano in the 17th century. The applied method to set up the sediment budget does not consider the deposits from this earlier eruption. It is possible that the hyperconcentrated and pyroclastic flows eroded ancient deposits from the 17th century eruption and transported them into the

delta. This would result in a negative storage value because the output volume could be larger than the input volume. Even if the equation can be solved without a negative storage it remains an uncertainty of the mass balance.

### Relevance

The 2008-2009 eruptive phase of the Chaitén volcano mobilized  $1.7 \pm 1.3 \cdot 10^7 \text{ m}^3$  volcaniclastic sediments within 8 years. By taking the grain density of  $1970 \pm 120 \text{ kg m}^{-3}$  and the catchment area of  $77 \text{ km}^2$  into account follows a specific sediment yield of  $5.4 \pm 0.5 \cdot 10^4 \text{ t km}^{-2} \text{ yr}^{-1}$ . The error range is based on the error from total inflow and the error of the grain densities. Major et al. (2000) provides a data collection of sediment fluxes following explosive eruptions of 13 volcanos within the last 100 years in 34 different valleys. The annual sediment yields of this eruptions range in order of magnitudes between  $10^3 \text{ t km}^{-2} \text{ yr}^{-1}$  and  $10^5 \text{ t km}^{-2} \text{ yr}^{-1}$ .

Korup (2012) reviewed some of the highest reported specific sediment yields in mountain rivers over timescales of  $10^{-4}$  to  $10^4$  years. Fluxes exceeding the 95th percentile have been defined as extreme events. Figure 2 shows that the highest recorded sediment yields occurred as a result of volcanic eruptions and range in magnitude of orders between  $10^4 \text{ t km}^{-2} \text{ yr}^{-1}$  and  $> 10^6 \text{ t km}^{-2} \text{ yr}^{-1}$ . The data collection of Major et al. (2000) seems to be focused on extraordinary large fluxes because 80% (including Chaitén) of the compiled data shows values greater  $10^4 \text{ t km}^{-2} \text{ yr}^{-1}$ . Nevertheless, the averaged specific sediment yield of Chaitén can barely defined as an extreme event.

Post-eruption sediment yields peak during the first three years after an eruption and decline rapidly after five to ten years (Ferrucci et al., 2005; Lavigne, 2004). The DGPS data showed that the volcaniclastic deposits are volumetrically decreasing even if there is still sediment accumulated within the catchment. Assuming that the loss of volume is mainly controlled by erosional processes, it can be concluded that erosion rates are greater than sedimentation rates. To make a statement regarding the persistence time of the delta it has furthermore to be assumed that erosional processes remain cyclic on a moderate-term timescale (e.g. tides, waves, rainfall and wind). The Chaitén delta would persist  $14 \pm 3$  years assuming that compaction does not play a significant roll. In this case the change from 2014 to 2015 would represent every years change. The rate of erosion can be compromised by various factors like growing vegetation which reduces the erodibility of sediments, discrete events like earthquakes or wildfires that can increase the rate of erosion but also deliver additional sediments, the anthropogenic impact due to manipulation of the fluvial system, etc. A prediction based on the DGPS data is not very reliable because neither the erosion processes have been quantified nor the rate of possible compaction could be determined.

Literature provides little information about volcaniclastic deltas. The behavior in terms of erosional modification of such fan deltas should be different than in quartzo-feldspatic based deltas due to density differences of the material. Syvitski (2005) showed that delta

sizes scale with the size of delivery system by analysing 55 deltas worldwide. The sediment source is not part of the discussion in this study. This leads to the question whether volcaniclastic deltas behave different as conventional deltas.

A Google Satellite Image from 2016 was used to locate fan deltas in southern Chile. The area of the 16 largest deltas between Valdivia and La Junta have been measured by using the open source program QGIS. The related drainage basin of these deltas have been calculated by applying remote sensing techniques on an open source ASTER 90m digital elevation model. The location of Chilean volcanoes of this area were downloaded from the database of the *Global Volcanism Program* (Smithsonian Institution, 2013). Figure 29 shows the results of this analysis in a bubble scatterplot. The color of the points shows whether there is a volcano in the particular catchment or not. The scale size of the points indicates the period of the last eruption. Basically the information confirms the analysis of (Svitski, 2005). Only the volcano Calbuco shows a much larger delta in relation to the catchment. The Calbuco erupted recently in late 2015, thus this delta could be an indication of a short persistence time of volcaniclastic deltas. More data of recent delta formation following volcanic eruptions would be necessary to obtain evidence for this hypothesis.

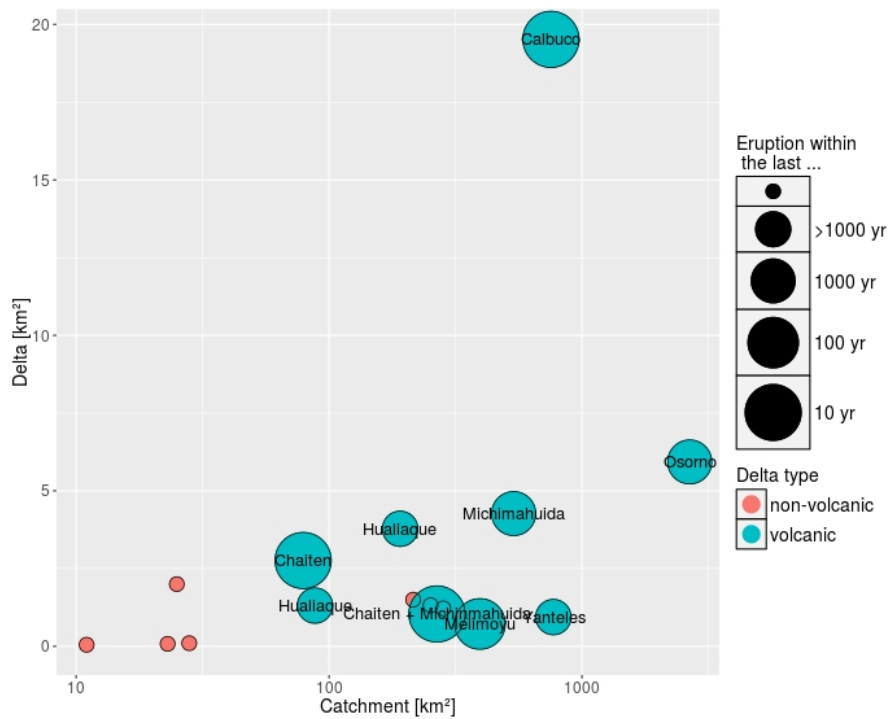


**Figure 29:** Relation of delta area to catchment area with volcanic activity

The volcaniclastic delta caused by the eruption of the Calbuco volcano suggests that such fan deltas rapidly regress into the catchment-scale related size within a short-term time scale. Nevertheless many factors are influencing the development of large sediment input fan deltas. It is doubtful that general statements regarding the evolution of volcaniclastic fan deltas can be done without detailed knowledge of the field conditions.

## 6 Conclusion

The aim of the study was to quantify the annual volumetric change of the Chaitén delta and to set up a simplified sediment budget of the volcaniclastic sediments mobilized by post-eruptive surface processes. The hypothesis that the Chaitén delta is still growing was falsified by analysing the DGPS data of two field trips in 2014 and 2015. Erosional processes of the delta are more dominant than the ongoing sediment supply from depositional terraces within the catchment. The presence of the longshore dune and the results of the grain size analysis show that the highly erodible volcaniclastic sediments get strongly modified by tides and waves. Proximal and distal differences in statistical grain size parameters have confirmed the influence of erosion.

The research questions can be answered by the following summarised results:

- I The annual volumetric change between 2014 and 2015 shows a decrease of  $7.8 \pm 2.5 \cdot 10^5 \text{ m}^3$  or  $1.53 \pm 0.6 \cdot 10^6 \text{ t}$ . The average lowering rate of the Chaitén delta is  $257 \pm 80 \text{ mm yr}^{-1}$ . Compaction driven subsidence is unlikely but can't be excluded on basis of the DGPS data.
- II The negative skewness and the small variance in sorting of the grain size analysis from the longshore samples indicates that wave and tide erosion lead to the surface reduction of this region. Low values of kurtosis confirms the tidal influence. The catchment samples are more positively skewed than the delta plane samples and suggest that fine grained material was directly transported into the ocean basin before accumulating on the delta.
- III The Chaitén delta will persist around  $14 \pm 3$  years, assuming that compaction-driven subsidence does not play a significant roll and erosional processes remain cyclic.
- IV Sediment storage of  $0.3 \pm 1.3 \cdot 10^7 \text{ m}^3$  was calculated by using an estimated sediment input of  $2 \cdot 10^7 \text{ m}^3$  from literature and a calculated sediment output of  $1.7 \pm 1.3 \cdot 10^7 \text{ m}^3$ . The negative storage within the error range could be explained by the erosion of ancient volcaniclastic deposits.
- V The specific sediment yield is  $5.4 \pm 0.5 \text{ t km}^{-2} \text{ yr}^{-1}$ . The sedimentary response to the 2008 eruption can be barely classified as an extreme event.

Volcaniclastic fan deltas can form following large inputs of tephra by volcanic eruptions close to shorelines or lakes. The amount of sediment, the grain sizes and the amount of water determine the sediment concentration of the resulting flow type. Density currents in the transition from debris flows to hyperconcentrated flows can reach regions far distant from the volcano and are highly hazardous. Deposits within the catchment can be mobilized years after an eruption and rain-triggered lahars can occur. The high erodibility of low

density tephra causes a rapid regress of such fan deltas. A general prediction of the persistence time of volcaniclastic deltas is not possible because the boundary conditions (e.g. bathymetry, ocean currents, rainfall, tides) of the environment are necessary. A stable volcaniclastic fan delta on a long-term scale is unlikely because the rate of sediment supply had to balance the rate of erosion. Furthermore the both rates had to be very small because sediment supply results from deposits within the catchment. The persistence for a moderate-term time scale is possible. The study shows that the Chaitén delta is still existing after eight years but also that the annual denudation totals in an order of magnitude of  $10^5 \text{ m}^3$ .

Further studies on the development of the Chaitén delta could be to measure time series of the subaqueous delta slope geometry and detect whether ocean currents and tidal energy erode the slope in a significant way or not. However, further studies with the objective to predict a reliable persistence time of the delta need to find evidence for possible compaction-driven subsidence.

For general studies on volcaniclastic deltas it would be reasonable to find ancient fan deltas or at least remains of them by using remote sensing techniques and conduct age dating of the deposits. The database of the Global Volcanism Program from the Smithsonian Institute could provide informations about possible locations. Sediment samples give information about the origin of the material and a geochemical analysis could try to find evidence for a possible relation of delta persistence and eruption type.

## References

- Alfano, F., Bonadonna, C., Volentik, A. C., Connor, C. B., Watt, S. F., Pyle, D. M., and Connor, L. J. (2011). Tephra stratigraphy and eruptive volume of the may, 2008, chaitén eruption, chile. *Bulletin of Volcanology*, 73(5):613–630.
- Branney, M. J. and Kokelaar, B. P. (2002). *Pyroclastic density currents and the sedimentation of ignimbrites*.
- Catuneanu, O. (2006). *Principles of sequence stratigraphy*. Elsevier.
- Encinas, A., Pérez, F., Nielsen, S. N., Finger, K. L., Valencia, V., and Duhart, P. (2014). Geochronologic and paleontologic evidence for a pacific–atlantic connection during the late oligocene–early miocene in the patagonian andes (43–44s). *Journal of South American Earth Sciences*, 55:1 – 18.
- Erban, L. E., Gorelick, S. M., and Zebker, H. A. (2014). Groundwater extraction, land subsidence, and sea-level rise in the mekong delta, vietnam. *Environmental Research Letters*, 9(8):084010.
- Ferrucci, M., Pertusati, S., Sulpizio, R., Zanchetta, G., Pareschi, M., and Santacroce, R. (2005). Volcaniclastic debris flows at la fossa volcano (vulcano island, southern Italy): Insights for erosion behaviour of loose pyroclastic material on steep slopes. *Journal of Volcanology and Geothermal Research*, 145(3-4):173–191.
- Fisher, R. V. and Schmincke, H.-U. (2012). *Pyroclastic rocks*. Springer Science & Business Media.
- Folk, R. L. and Ward, W. (1957). Brazos river bar: A study in the significance of grain size parameters. *Journal of sedimentary Petrology*.
- Friedman, G. M. (1962). On sorting, sorting coefficients, and the lognormality of the grain-size distribution of sandstones. *The Journal of Geology*, pages 737–753.
- Garreaud, R., Lopez, P., Minvielle, M., and Rojas, M. (2013). Large-scale control on the patagonian climate. *Journal of Climate*, 26(1):215–230.
- Higgins, S., Overeem, I., Tanaka, A., and Syvitski, J. P. M. (2013). Land subsidence at aquaculture facilities in the yellow river delta, China. *Geophysical Research Letters*, 40(15):3898–3902.
- Hinderer, M. (2012). From gullies to mountain belts: a review of sediment budgets at various scales. *Sedimentary Geology*, 280:21–59.
- Jothiprakash, V. and Garg, V. (2008). Re-look to conventional techniques for trapping efficiency estimation of a reservoir. *International Journal of Sediment Research*, 23(1):76–84.

- Korup, O. (2012). Earth's portfolio of extreme sediment transport events. *Earth-Science Reviews*, 112(3):115–125.
- Lara, L. E. (2009). The 2008 eruption of the chaitén volcano, chile: a preliminary report. *Andean Geology*, 36(1):125–129.
- Lara, L. E., Moreno, R., Amigo, Á., Hoblitt, R. P., and Pierson, T. C. (2013). Late holocene history of chaitén volcano: New evidence for a 17th century eruption. *Andean Geology*, 40(2):249–261.
- Lavigne, F. (2004). Rate of sediment yield following small-scale volcanic eruptions: a quantitative assessment at the merapi and semeru stratovolcanoes, java, Indonesia. *Earth Surface Processes and Landforms*, 29(8):1045–1058.
- Lavigne, F. and Thouret, J.-C. (2003). Sediment transportation and deposition by rain-triggered lahars at merapi volcano, central java, Indonesia. *Geomorphology*, 49(1-2):45–69.
- Luo, W., Taylor, M., and Parker, S. (2008). A comparison of spatial interpolation methods to estimate continuous wind speed surfaces using irregularly distributed data from england and wales. *International Journal of Climatology*, 28(7):947–959.
- Major, J. J. and Lara, L. E. (2013). Overview of chaitén volcano, chile, and its 2008-2009 eruption. *Andean Geology*, 40(2):196–215.
- Major, J. J., Pierson, T., Dinehart, R., and Costa, J. (2000). Sediment yield following severe volcanic disturbance—a two-decade perspective from mount st. helens. *Geology*, 28(9):819–822.
- Major, J. J., Pierson, T. C., Hoblitt, R. P., and Moreno, H. (2013). Pyroclastic density currents associated with the 2008-2009 eruption of chaitén volcano (chile): Forest disturbances, deposits, and dynamics. *Andean Geology*, 40(2):324–358.
- Manville, V., Németh, K., and Kano, K. (2009). Source to sink: a review of three decades of progress in the understanding of volcaniclastic processes, deposits, and hazards. *Sedimentary Geology*, 220(3):136–161.
- Manville, V., White, J., Houghton, B., and Wilson, C. (1998). The saturation behaviour of pumice and some sedimentological implications. *Sedimentary Geology*, 119(1–2):5 – 16.
- Pallister, J. S., Major, J. J., Pierson, T. C., Hoblitt, R. P., Lowenstern, J. B., Eichelberger, J. C., Lara, L., Moreno, H., Muñoz, J., Castro, J. M., et al. (2010). Interdisciplinary studies of eruption at chaitén volcano, chile. *Eos, Transactions American Geophysical Union*, 91(42):381–382.
- Pierson, T. C. (2005). Hyperconcentrated flow—transitional process between water flow and debris flow. In *Debris-flow hazards and related phenomena*, pages 159–202. Springer.

## REFERENCES

---

- Pierson, T. C., Janda, R. J., Umbal, J. V., and Daag, A. S. (1992). *Immediate and long-term hazards from lahars and excess sedimentation in rivers draining Mt. Pinatubo, Philippines*. US Department of the Interior, US Geological Survey.
- Pierson, T. C. and Major, J. J. (2014). Hydrogeomorphic effects of explosive volcanic eruptions on drainage basins\*. *Annual Review of Earth and Planetary Sciences*, 42:469–507.
- Pierson, T. C., Major, J. J., Amigo, Á., and Moreno, H. (2013). Acute sedimentation response to rainfall following the explosive phase of the 2008–2009 eruption of chaitén volcano, chile. *Bulletin of Volcanology*, 75(5):1–17.
- Postma, G. (1990). An analysis of the variation in delta architecture. *Terra Nova*, 2(2):124–130.
- Rajganapathi, V. C., Jitheshkumar, N., Sundararajan, M., Bhat, K. H., and Velusamy, S. (2012). Grain size analysis and characterization of sedimentary environment along thiruchendur coast, tamilnadu, India. *Arab J Geosci*, 6(12):4717–4728.
- Rogers, J. J. and Head, W. B. (1961). Relationships between porosity, median size, and sorting coefficients of synthetic sands. *Journal of Sedimentary Research*, 31(3).
- Sadler, P. M. and Jerolmack, D. J. (2015). Scaling laws for aggradation, denudation and progradation rates: the case for time-scale invariance at sediment sources and sinks. *Geological Society, London, Special Publications*, 404(1):69–88.
- Servicio Nacional de Geología y Minería, Carta Geológico de Chile, S. (2002). Mapa geológico de chile. *Serie Geología Basica, 1 mapa en 3 hojas, escala 1:1000000*, 1(No. 75):1.
- Siebert, L. (2002). Landslides resulting from structural failure of volcanoes. *Reviews in Engineering Geology*, 15:209–235.
- Slaymaker, O. (2003). *The Interactions between Sediments and Water: Proceedings of the 9th International Symposium on the Interactions between Sediments and Water, held 5-10 May 2002 in Banff, Alberta, Canada*, chapter The sediment budget as conceptual framework and management tool, pages 71–82. Springer Netherlands, Dordrecht.
- Smithsonian Institution (2013). Volcanoes of the world. *Global Volcanism Program*. Downloaded 14 February 2016.
- Stuut, J., Marchant, M., Kaiser, J., Lamy, F., Mohtadi, M., Romero, O., and Hebbeln, D. (2006). The late quaternary paleoenvironment of chile as seen from marine archives. *Geographica Helvetica*, 61(2):135.
- Syvitski, J. P. (2005). The morphodynamics of deltas and their distributary channels. *River, Coastal, and Estuarine Morphodynamics*, pages 143–150.

## REFERENCES

---

- Umazano, A. M., Melchor, R. N., Bedatou, E., Bellosi, E. S., and Krause, J. M. (2014). Fluvial response to sudden input of pyroclastic sediments during the 2008–2009 eruption of the chaitén volcano (Chile): The role of logjams. *Journal of South American Earth Sciences*, 54:140–157.
- Vallance, J. W. and Iverson, R. M. (2015). Lahars and their deposits. *The Encyclopedia of Volcanoes*, page 649–664.
- Veblen, T., Young, K., and Orme, A. (2015). *The Physical Geography of South America*. Oxford Regional Environments. Oxford University Press.
- Verstraeten, G. and Poesen, J. (2000). Estimating trap efficiency of small reservoirs and ponds: methods and implications for the assessment of sediment yield. *Progress in Physical Geography*, 24(2):219–251.
- Wang, C.-y., Cheng, L.-H., Chin, C.-V., and Yu, S.-B. (2001). Coseismic hydrologic response of an alluvial fan to the 1999 chi-chi earthquake, taiwan. *Geology*, 29(9):831–834.
- Whelley, P. L., Jay, J., Calder, E. S., Pritchard, M. E., Cassidy, N. J., Alcaraz, S., and Pavez, A. (2011). Post-depositional fracturing and subsidence of pumice flow deposits: Lascar volcano, Chile. *Bull Volcanol*, 74(2):511–531.

## **APPENDIX**

## **A Programming code in R**

The programming scripts are uploaded to an open source repository on github.com

[https://github.com/deniztg/chaiten\\_chile](https://github.com/deniztg/chaiten_chile)

Please download the files to execute the R scripts. The necessary data files are also uploaded but password protected.

Password: delta\_force

## B Figures

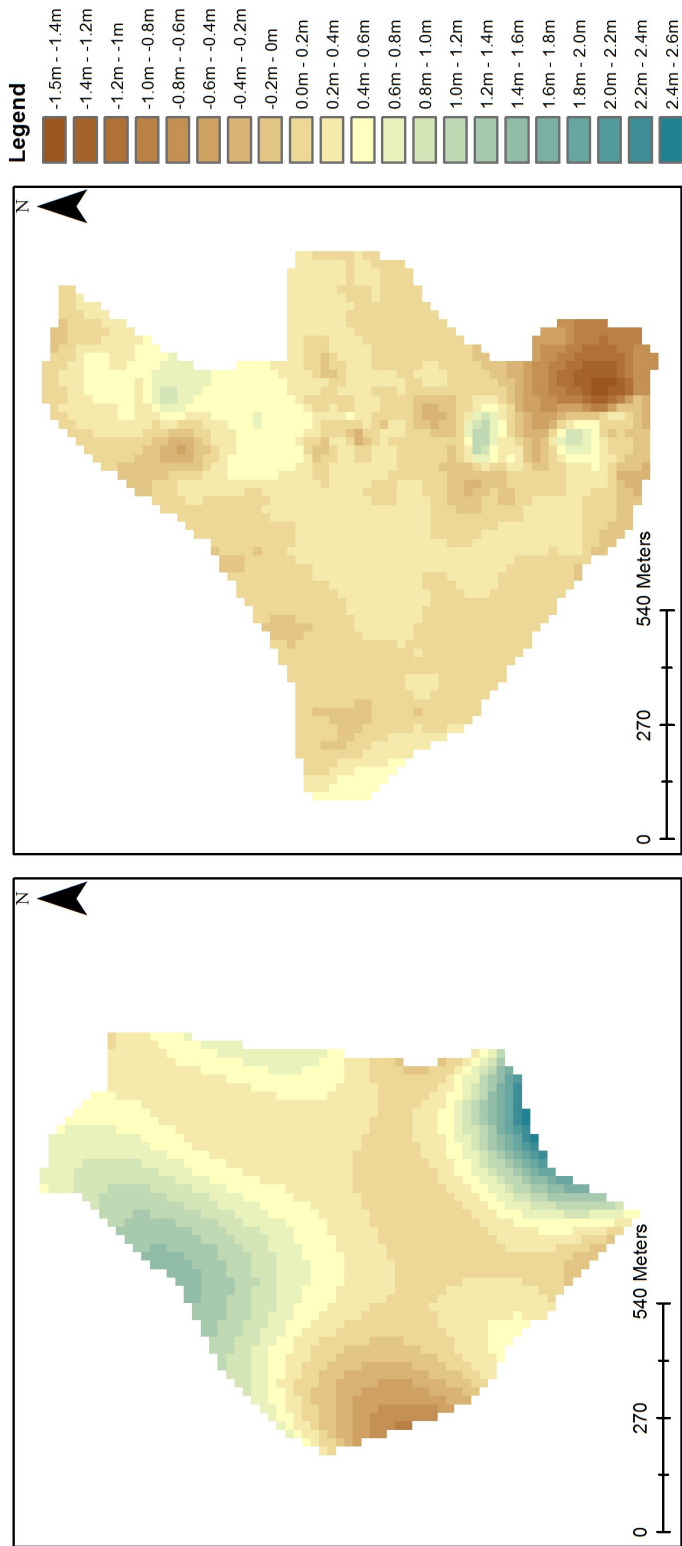


**Figure 30:** Elevation difference of the interpolated DGPS data. Negative values represent elevation increase, positive values elevation decrease in meters.

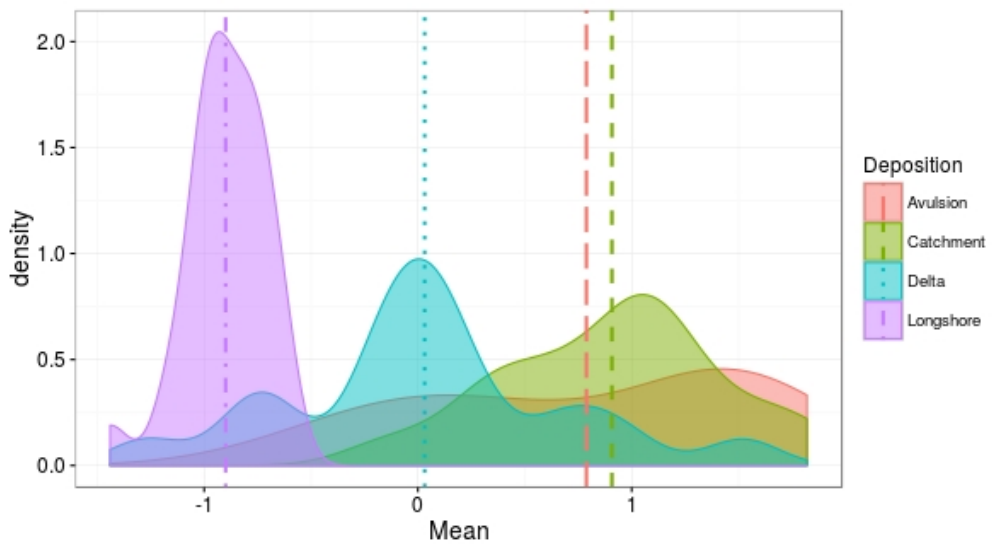


**Figure 31:** Density plot of the statistical parameters mean

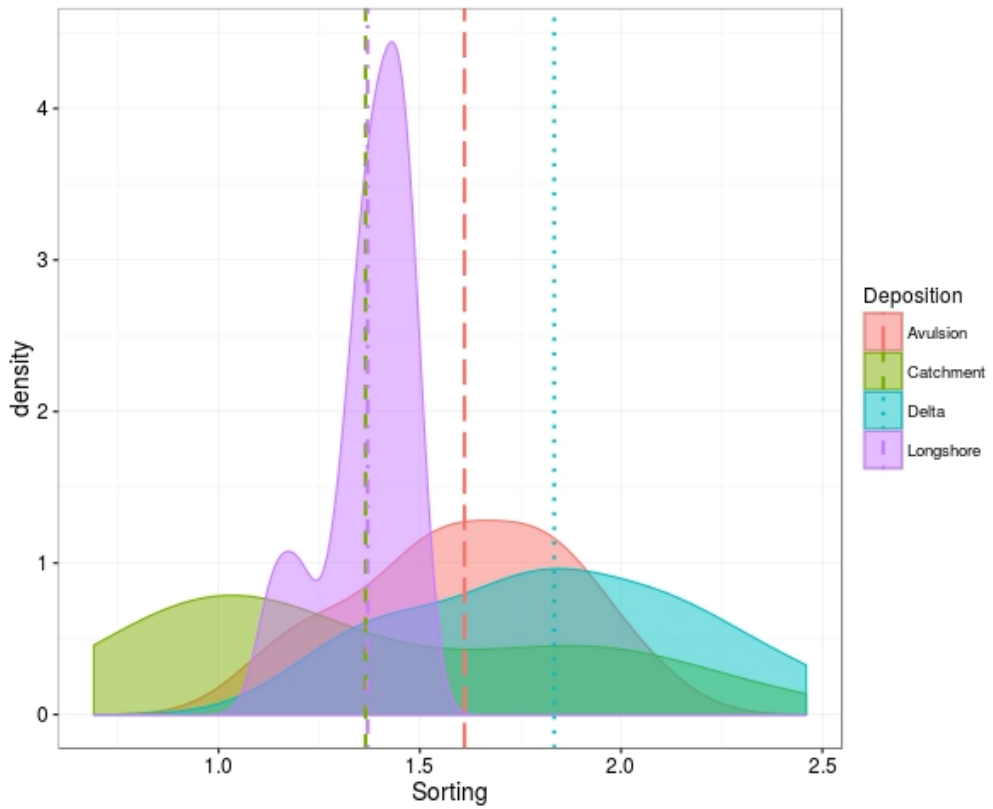


**Figure 32:** Density plot of the statistical parameter sorting

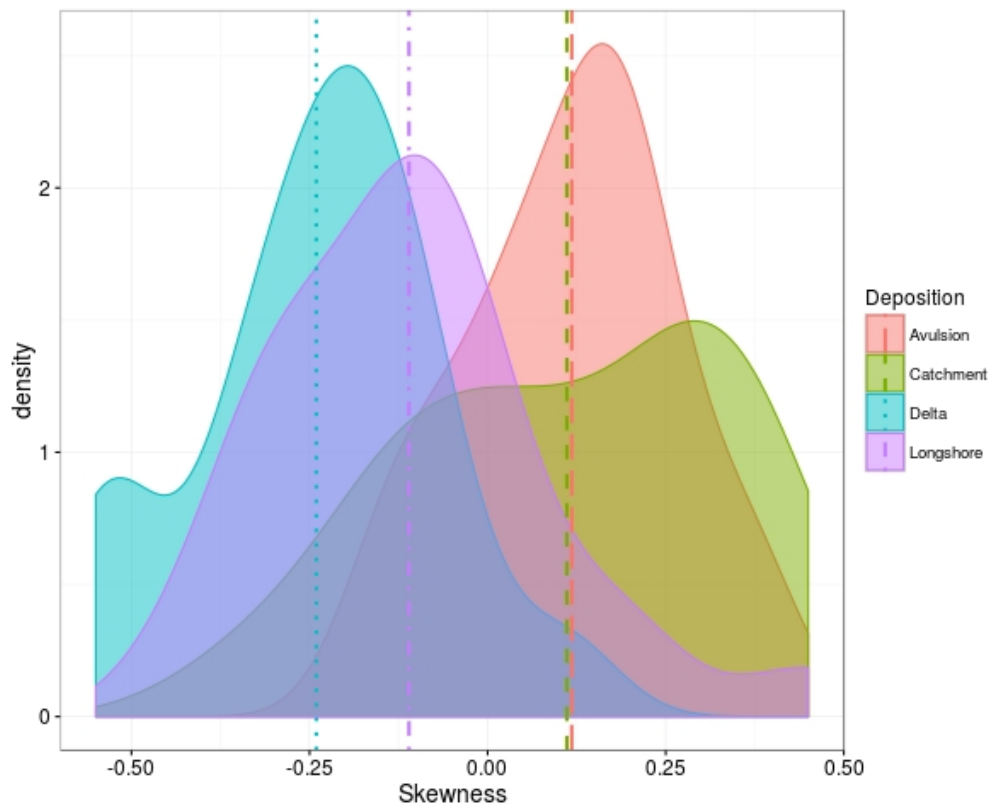


**Figure 33:** Density plot of the statistical parameter skewness

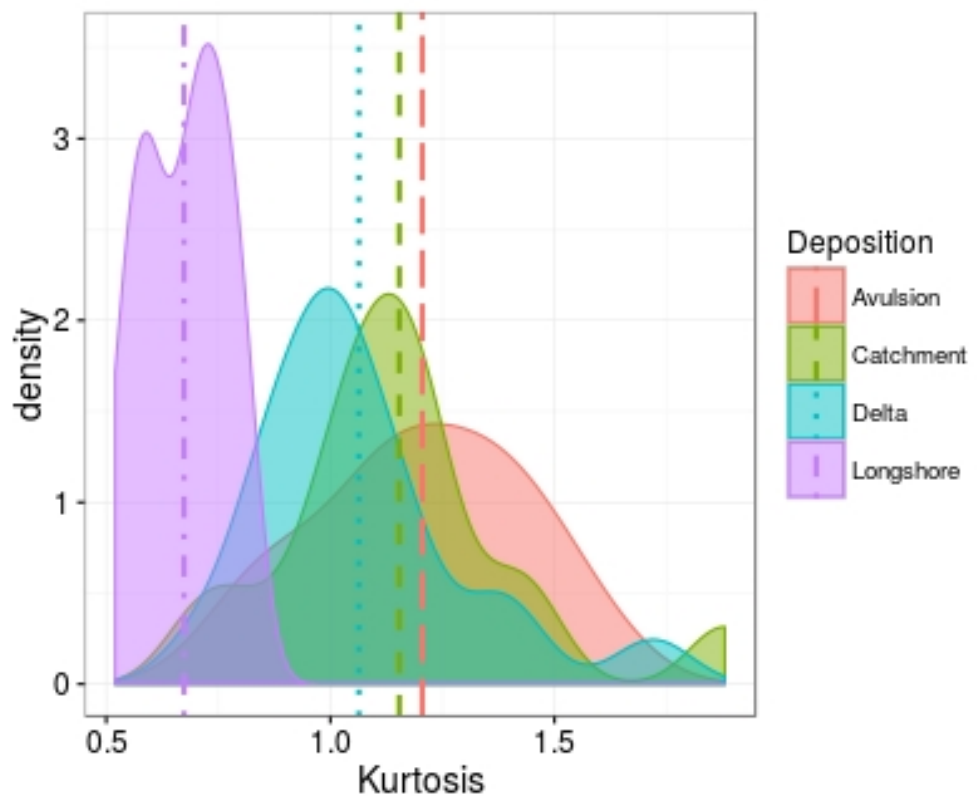


**Figure 34:** Density plot of the statistical parameter kurtosis



**Figure 35:** Greenschist bed load sample



**Figure 36:** Granodiorite bed load sample



**Figure 37:** Rhyolite bed load sample

## C Data of delta comparision

**Table 9:** Data of different deltas in southern Chile (Fig. 29)

Delta	Delta km <sup>2</sup>	Watershed km <sup>2</sup>	Volcano	Latitude	Longitude
Delta 1	0.08	23	no volcano	-73.3828425	-39.94341
Delta 2	1.22	283	no volcano	-73.5844278	-39.95137
Delta 3	0.1	28	no volcano	-73.7426006	-40.60437
Delta 4	0.05	11	no volcano	-73.7537397	-40.61638
Delta 5	2	25	no volcano	-73.6463368	-41.56128
Delta 6	19.52	754	Calbuco	-72.8135447	-41.50981
Delta 7	5.93	2667	Osorno	-72.3101852	-41.38903
Delta 8	1.31	88	Hualiaque	-72.7168526	-41.79630
Delta 9	3.78	191	Hualiaque	-72.6623745	-42.00903
Delta 10	1.32	252	no volcano	-72.4378225	-41.97151
Delta 11	1.5	215	no volcano	-72.3879149	-42.25416
Delta 12	4.27	537	Michimahuida	-72.5201436	-42.58178
Delta 13	1.04	267	Michinmahuida	-72.8495633	-42.76294
Delta 14	2.76	79	Chaiten	-72.7194583	-42.91991
Delta 15	0.94	771	Yanteles	-72.9479757	-43.63976
Delta 16	0.72	395	Melimoyu	-73.0941497	-44.08740

## D Grain size data

**Table 10:** General information of sediment sampling

Depositional environment	Sample name	Latitude	Longitude	Date of sampling
Longshore	LS01	-72.72238	-42.918227	07.02.15
Longshore	LS02	-72.721331	-42.916723	07.02.15
Longshore	LS03	-72.71974	-42.915139	07.02.15
Longshore	LS04	-72.71831	-42.913966	07.02.15
Longshore	LS05	-72.717274	-42.913084	07.02.15
Pre-eruption channel	AV01	-72.42819	-42.55719	06.02.14
Pre-eruption channel	AV02	-72.42787	-42.55844	06.02.14
Pre-eruption channel	AV03	-72.42902	-42.55928	06.02.14
Pre-eruption channel	AV04	-72.43087	-42.55590	06.02.14
Pre-eruption channel	AV05	-72.43221	-42.55935	06.02.14
Pre-eruption channel	AV06	-72.43322	-42.55974	06.02.14
Pre-eruption channel	AV07	-72.43301	-42.56003	06.02.14
Pre-eruption channel	AV08	-72.43177	-42.56008	06.02.14
Pre-eruption channel	AV09	-72.42727	-42.55700	06.02.14
Pre-eruption channel	AV10	-72.42593	-42.55765	06.02.14
Catchment	Teph05 -1	-72.6925	-42.8984	08.02.2015 / 10.02.2015
Catchment	Teph05 -2	-72.6925	-42.8984	08.02.2015 / 10.02.2015
Catchment	Teph05 -3	-72.6925	-42.8984	08.02.2015 / 10.02.2015
Catchment	Teph05 -4	-72.6925	-42.8984	08.02.2015 / 10.02.2015
Catchment	Teph05 -5	-72.6925	-42.8984	08.02.2015 / 10.02.2015
Catchment	Teph03-1	-72.6936	-42.9045	08.02.2015 / 10.02.2015
Catchment	Teph03-2	-72.6936	-42.9045	08.02.2015 / 10.02.2015
Catchment	Teph03-3	-72.6936	-42.9045	08.02.2015 / 10.02.2015
Catchment	Teph03-4	-72.6936	-42.9045	08.02.2015 / 10.02.2015
Catchment	Teph03-5	-72.6936	-42.9045	08.02.2015 / 10.02.2015
Catchment	Teph07-1	-72.6889	-42.8853	08.02.2015 / 10.02.2015
Catchment	Teph07-2	-72.6889	-42.8853	08.02.2015 / 10.02.2015
Catchment	Teph07-3	-72.6889	-42.8853	08.02.2015 / 10.02.2015
Delta plane	Val11	-72.718409	-42.920845	26.03.13
Delta plane	Val12	-72.715555	-42.920955	26.03.13
Delta plane	Val15	-72.714868	-42.921504	26.03.13
Delta plane	Val10	-72.72034	-42.920876	26.03.13
Delta plane	Val01	-72.713656	-42.921269	26.03.13
Delta plane	Val03	-72.714428	-42.920938	26.03.13
Delta plane	Val05	-72.713774	-42.916854	26.03.13
Delta plane	Val04	-72.713752	-42.915707	26.03.13
Delta plane	Val02	-72.714438	-42.921331	26.03.13
Delta plane	Val06	-72.713838	-42.919588	26.03.13
Delta plane	Val07	-72.718258	-42.917624	26.03.13
Delta plane	Val08	-72.717164	-42.918441	26.03.13
Delta plane	Val13	-72.719148	-42.92330	26.03.13
Delta plane	Val14	-72.717636	-42.922736	26.03.13
Delta plane	chtn	-72.713642	-42.9209212	26.03.13
Delta plane	N1	-72.713784	-42.918317	26.03.13
Delta plane	NW1	-72.716122	-42.919196	26.03.13
Delta plane	W1	-72.716895	-42.92092	26.03.13
Delta plane	SW1	-72.716251	-42.922073	26.03.13

## D GRAIN SIZE DATA

---

**Table 11:** Sample mass and sieving loss

Sample name	Sediment mass [g]	Sieving loss [g]	Sample name	Sediment mass [g]	Sieving loss [g]
LS01-1	1385,69	1,75	Goek AV07	840	5,27
LS01-2	1186,51	0,41	Goek AV04	852,8	3
LS01-3	1610,08	2,5	Goek AV02	914,9	3,5
LS01-4	985,28	0,41	Goek AV09	1008,6	1,1
LS01-5	1466,73	2,69	Goek AV03	1058,9	1,5
LS02-1	1326,48	3	Goek AV08	802,4	6,4
LS02-2	1438,57	1,95	Goek AV10	812,7	6,7
LS03-3*	1860,59	0,8	Goek AV05	801,2	5,5
LS02-4	1358,84	1,34	Goek AV01	929,5	5,7
LS02-5	1235,66	0,07	Goek AV06	678,1	5,5
LS03-1	1264,39	2,23	Teph03(1)	1204,99	-292,53
LS03-2	1456,1	1,97	Teph03(2)	785,67	0,02
LS03-3	1202,66	1,11	Teph03(3)	1256,08	0,89
LS03-4	1445,25	2,3	Teph03(4)	1144,25	0,3
LS03-5	1193,37	0,7	Teph03(5)	1485,99	3,5
LS04-1	1101,03	0,6	Teph05(1)	1149,84	0,87
LS04-2	1193,75	1,2	Teph05(2)	1197,96	1,46
LS04-3	1165,12	0,6	Teph05(3)	1061,87	0,19
LS04-4	1354,84	2,01	Teph05(4)	1218,55	-727,46
LS04-5	1285,61	1,88	Teph05(5)	1002,99	0,11
LS05-1	1465,19	0,99	Teph07(1)	684,49	0,7
LS05-2	1270,84	0,6	Teph07(2)	1277,44	1,3
LS05-3	1160,64	0,88	Teph07(3)	1165,86	0,4
LS05-4	1149,51	1,3	Teph09(1)	830,82	0,24
LS05-5	1119,04	1,35	Teph09(2)	1199,69	1,03
Val06	368,58	1,13	Teph09(3)	833,26	0,22
N1	550,06	-0,49			
Val05	369,24	2,03			
Val04	392,72	2,22			
Val09	356,45	5,07			
NW1	564,19	3,22			
Val08	347,96	1,57			
Val07	389,59	2,71			
Val12	398,35	0,56			
W1	767,26	2,83			
Val11	365,78	0,81			
Val10	406,96	1,54			
Val15	324,04	1,5			
SW1	528,26	1,65			
Val13	283,6	1,65			

**Table 12:** Grain size data of the 2013 delta samples

Sample	Meshsizes (mm)	30	20	10	6,3	4	3,15	2	1,25	1	0,6	0,43	0,4	0,25	0,21	0,13	0,063	0
val01	0	12,19	70,32	39,04	0	59,13	29,99	37,16	0	59,89	0	32,85	22,14	0	12,38	3,53	1,45	
val02	0	0	12,31	11,14	0	36,31	36,36	61,13	0	131,57	0	72,41	24,88	0	5,86	1,15	0,37	
val03	0	0	0	3,67	0	10,99	10,02	19,29	0	59,56	0	3,73	80,23	0	76,06	24,78	6,16	
val04	0	8,77	8,99	26,46	0	42,24	35,72	49,98	0	93,78	0	59,49	40,66	0	18,68	4,49	2,14	
val05	0	12,26	43,93	23,86	0	52,59	29,46	35,74	0	63,55	0	43,77	36,33	0	19,65	4,37	1,7	
val06	0	0	25,04	10,33	0	28	27,01	44,32	0	89,79	0	58,9	42,42	0	23,66	8,37	9,61	
val07	0	8,31	13,81	10,6	0	14,47	11,58	20,85	0	60,05	0	92,6	99,73	0	45,91	7,42	1,55	
val08	0	13,65	7,85	7,23	0	17,64	15,29	25,89	0	70,18	0	76,17	64,7	0	38,4	7,71	1,68	
val09	0	0	1,21	5,93	0	22,25	27,18	48,43	0	120,38	0	54,41	44,34	0	21,14	4,89	1,22	
val10	0	7,04	44,48	28,22	0	51,37	35,21	48,55	0	89,22	0	50,88	29,07	0	14,83	5,74	0,81	
val11	0	0	5,34	11,03	0	31,75	30,96	49,98	0	100,68	0	64,79	42,92	0	20,11	5,7	1,71	
val12	0	16,03	28,22	18,8	0	36,91	33,05	54,28	0	104,12	0	50,37	27,31	0	17,37	8,37	2,96	
val13	0	0	0	2,63	0	14,87	10,65	17,99	0	49,83	0	71,32	71,59	0	36,12	5,92	1,2	
val15	0	34,74	17,95	14,55	0	31,78	25,58	36,64	0	67,78	0	38,55	24,02	0	13,71	7,25	9,99	
n1	0	51,41	24,89	15,5	19,27	0	31,06	0	62,77	74,8	76,45	0	0	117,52	41,38	23,48	12,02	
nw1	0	0	30,83	32,04	24,21	40,44	0	81,3	0	65,02	65,32	164,09	0	0	40,25	11,35	6,14	
w1	0	0	51,17	43,49	52,56	0	115,91	0	175,3	106,37	66,64	0	0	89,31	29,51	20,39	13,78	
sw1	0	15,65	36,47	29,2	40,88	0	74,49	0	96,52	86,68	55,36	0	0	60,43	16,18	7,04	7,71	
start	0	3,05	23,56	19,51	0	36,4	35,06	57,53	0	90,29	0	63,3	60,32	0	33,04	11,06	2,93	

**Table 13:** Grain size data of the 2014 pre-eruption samples

Sample	Meshsizes (mm)	20	10	6,3	3,15	1	0,6	0,4	0,32	0,21	0,13	0,063	0
AV01	0,1	7,2	18,1	74,7	314,1	87,1	73,3	161,1	79,4	33,4	26,5	48,9	
AV02	0,1	3	5,1	39,9	466,9	131,2	73,6	40	47,9	33,4	28,9	41,5	
AV03	0	0	0,7	2,2	60,9	161,9	202,3	161,2	212,9	129,6	68,8	56,9	
AV04	0	0	1,6	9,9	122,6	129,6	113	91,1	151,3	111,8	70,3	48,6	
AV05	0	0	0,4	8,1	102,7	138,2	125,3	84,7	127,1	87,2	62,5	59,5	
AV06	0	3,9	6,7	40,5	428,3	107,6	25,4	10,8	16	12,8	11,8	8,8	
AV07	0	0,33	30,8	128,7	362,3	66,9	37,2	32,5	72,3	66,2	29	8,5	
AV08	0	0	2,8	17,3	88,8	104,2	100	76,8	159,3	138,4	71,8	36,6	
AV09	0	0	1,1	15,2	240	280,4	176,6	76,3	82,2	51,1	36,5	48,1	
AV10	0	2	7,2	26,1	215,1	69,4	45,5	85,1	96,7	114,7	96,3	47,9	

Table 14: Grain size data of the 2015 catchment samples

Meshsizes (mm)	20	10	6,3	4	2	1	0,6	0,43	0,21	0,13	0,08	0,06	0
Teph03(1)	0	0	297	31,53	184,89	159,11	381,99	100,89	101,19	44,24	59,36	88,94	48,38
Teph03(2)	0	0	10,47	31,9	151,6	127,58	127,18	76,42	82,62	44,06	82,1	37,93	13,79
Teph03(3)	0	0	1,23	9,89	72,31	171,99	488,97	127,21	131,2	76,17	115,84	48,19	12,19
Teph03(4)	0	0	62,13	67,97	149,45	151,71	342,4	90,36	96,84	65,93	82,26	27,35	7,55
Teph03(5)	0	0	28,86	82,63	214,73	187,78	416,28	188,44	124,3	68,16	99,19	55,22	16,9
Teph05(1)	0	0	0,14	0,39	12,54	58,11	469,51	201,93	231,65	71,75	53,05	30,29	19,61
Teph05(2)	0	0	0	1,92	10,71	29,73	341,34	213,34	334,66	126,74	85,97	35,28	16,81
Teph05(3)	0	0	0	1,31	21,03	51,43	360,21	211,48	249,59	64,83	42,51	35,86	23,43
Teph05(4)	0	0	0	1,16	8,28	26,82	360,6	288,15	344,66	810,7	58,71	32,57	14,36
Teph05(5)	0	0	0	0	3,76	23,66	359,56	212,61	252,43	60,28	44,56	32,19	13,83
Teph07(1)	0	0	1,04	4,72	30,86	55,71	323,88	146,55	103,66	10,78	2,98	0,44	3,17
Teph07(2)	0	0	0	0,97	8,16	37,16	626,21	297,18	255,06	35,43	9,14	1,19	5,64
Teph07(3)	0	0	4,45	10,92	84,72	161,25	600,19	177,15	108,52	10,59	2,78	0,49	4,4
Teph09(1)	0	0	41,54	26,34	56,69	50,14	154,11	77,34	178,2	114,07	80,18	20,46	31,51
Teph09(2)	0	0	0,3	3,47	29,58	73,14	438,75	216,55	301,72	78,48	31,01	6,45	19,21
Teph09(3)	0	0	18,15	12,04	28,18	24,26	104,46	91,97	310,18	131,49	64,29	19,81	28,21

Table 15: Grain size data of the 2015 longshore samples

Sample	Meshsizes (mm)	6,3	4	2	1	0,6	0,43	0,21	0,13	0,08	0,063	0
LS01(1)	315,29	86,14	131,22	136,93	510,88	110,74	84,71	6,85	0,66	0,18	0,34	
LS01(2)	173,54	73,05	221,97	222,99	375,33	56,04	54,98	7,26	0,65	0,08	0,21	
LS01(3)	347,72	105,48	283,15	283,41	448,83	67,51	61,71	8,21	0,89	0,11	0,56	
LS01(4)	311,59	54,46	73,82	75,06	321,11	76,73	65,31	6,01	0,44	0,09	0,25	
LS01(5)	401,17	109,22	200,51	193,86	428,61	64,75	58,29	6,67	0,6	0,08	0,28	
LS02(1)	256,96	97,08	240,58	284,39	378,95	27,99	29,89	6,33	0,84	0,13	0,34	
LS02(2)	132,29	96,43	262,66	368,54	504,46	26,07	36,8	8,02	0,99	0,06	0,3	
LS02(3)	363,47	161,48	355,7	343,44	451,67	61,51	100,98	17,89	2,55	0,26	0,84	
LS02(4)	140,79	91,77	251,49	341,6	451,2	35,74	35,3	8,1	0,96	0,13	0,42	
LS02(5)	302,78	86,71	199,57	231,19	340,51	32,98	33,69	7,09	0,85	0,09	0,13	
LS03(1)	211,88	105,71	211,92	250,01	350,26	44,98	72,36	13,35	1,16	0,17	0,36	
LS03(2)	258,78	113,47	228,7	286,35	411,52	52,45	84,29	15,17	2,28	0,23	0,89	
LS03(3)	123,8	80,62	301,46	353,38	296,36	19,33	21,09	4,63	0,61	0,04	0,23	
LS03(4)	291,98	118,76	229,02	255,81	387	50,89	86,17	18,47	3,52	0,38	0,95	
LS03(5)	231,18	81,5	189,97	255,12	319,3	35,26	65,47	12,34	1,83	0,14	0,56	
LS04(1)	194,38	64,78	144,48	193,22	402,03	42,66	41,69	15,16	1,56	0,18	0,29	
LS04(2)	188,82	69,27	160,9	209,58	426,4	48,45	63,25	23,41	2,05	0,13	0,29	
LS04(3)	255,59	86,45	161,89	195,63	372,41	36,7	39,24	14,72	1,48	0,1	0,31	
LS04(4)	256,28	133,78	265,53	239,64	360,58	33,88	42,28	18,17	2,04	0,21	0,44	
LS04(5)	213,36	62,21	172,05	256,31	448,04	48,1	61,12	20,15	1,96	0,14	0,29	
LS05(1)	265,89	246,69	279,95	232,15	308,6	35,74	66,61	22,29	4,54	0,47	1,27	
LS05(2)	256,52	184,33	268,75	179,09	308,48	23,88	33,7	12,41	2,19	0,18	0,71	
LS05(3)	125,84	109,27	259,83	240,25	302,65	48,52	53,89	12,91	4,68	0,57	1,35	
LS05(4)	167,95	146,29	245,16	227,59	268,84	28,59	41,26	16,4	4,5	0,45	1,18	
LS05(5)	360,36	156,77	225,39	162	171,1	16,5	19,81	4,2	1,06	0,18	0,32	